Exploiting Interference With an Intelligent Reflecting Surface to Enhance Data Transmission

Zhao Li, *Member, IEEE*, Chengyu Liu, Lijuan Zhang, Kang G. Shin, *Life Fellow, IEEE*, Jia Liu, *Senior Member, IEEE*, Zheng Yan, *Fellow, IEEE*, and Riku Jäntti, *Senior Member, IEEE*

***Abstract*— With the increasing number of wireless devices connecting to networks and sharing spectrum resources, interference has become a major obstacle to improving network performance. Existing interference management (IM) methods treat interference as a negative factor and focus on suppressing or eliminating its impact on the transmission of intended signals. However, this often comes at the cost of consuming communication resources and degrading desired transmission performance. Therefore, the design of a cost-effective IM method that "exploits" interference is important. To achieve this goal, we propose *Intelligent Reflecting Surface Assisted Interference Exploitation* (IRS-IE) to realize efficient desired data transmission. `IRS-IE` leverages the low-cost and adaptive deployment capabilities of IRS to gather and reflect interference towards the interfered receiver (Rx). By appropriately designing the reflection coefficient of IRS, a phase shift is introduced to the incident interference, allowing the reflected interference to interact with its direct counterpart at the interfered Rx. As a result, the interfered Rx can retrieve its desired data from the mixed interference. This way, `IRS-IE` can make use of the interference to facilitate the desired data transmission. Our theoretical analysis and simulation results show that `IRS-IE` significantly improves the spectral efficiency (SE) of the interfered communication pair over the other IM methods.**

***Index Terms*— Intelligent reflecting surface, interference management, interference utilization, spectral efficiency.**

I. Introduction

As WIRELESS communication technologies continue to develop rapidly, the increasing number of subscribers and data services have made spectrum resources scarcer. Numerous spectrum-sharing mechanisms have thus been proposed to improve the efficiency of spectrum utilization. However, with the growing number of concurrent communications, interference has become a key impediment to network performance improvement [1]. Multi-antenna technology exploits array signal processing to allow communication devices to distinguish multiple signals and interferences in the spatial domain. This enables interference management (IM) through the design of directional beams and/or receive filters. Various IM methods have been developed, including successive interference cancellation (SIC) [2], [3], [4], zero-forcing beamforming (ZFBF) [5], interference alignment (IA) [6], and interference neutralization (IN) [7], etc.

IM can be realized either individually or jointly at the transmitter (Tx) and/or the Rx. However, all IM methods come with their own deficiency. For example, SIC suffers from error propagation as well as high Rx complexity. For ZFBF, precoding, while eliminating the effect of interference on the desired communication, also introduces the signal sent from the interfering source to its Rx (called the *interfering Rx*) to match its channel less effectively, thus weakening the desired signal strength at the interfering Rx [8]. That is, ZFBF is achieved at the expense of the performance of the interfering communication pair. IA suffers from similar problems as ZFBF, and the interfered Rx needs to consume an additional spatial degree of freedom (DoF) for placing the aligned interferences. Although IN need not consume the DoF at the interfered Rx, it consumes power for constructing and transmitting the neutralizing signal. Furthermore, there may be cases where IN is not available due to the limited transmit power when the interference strength is too high. In summary, SOTA (state of the art) IM methods cause some loss of signal quality or/and consumption of communication resources, such as power and DoF. It is, therefore, important to develop more efficient and cost-effective IM methods.

Since all signals are energy-carrying electromagnetic waves, it is worthwhile to explore whether the energy of interference can be collected and utilized to reduce the overhead of IM and facilitate the interfered communication pair's data transmission. The authors of [9] employed an IRS to backscatter the jamming signal into the desired signal to enhance the reception quality for the user. In [10], interferences are categorized into constructive and destructive types. Subsequently, partial channel inversion is employed to preserve and leverage constructive interference, while effectively mitigating the

Manuscript received 25 July 2023; revised 6 November 2023 and 16 January 2024; accepted 7 February 2024. Date of publication 23 February 2024; date of current version 14 August 2024. This work was supported in part by the National Natural Science Foundation of China under Grant 62072351 and Grant U23A20300; in part by the Key Research Project of Shaanxi Natural Science Foundation under Grant 2023-JC-ZD-35; in part by the Open Research Project of Zhejiang Laboratory under Grant 2021PD0AB01; in part by the 111 Project under Grant B16037; in part by the Academy of Finland under Grant 308087, Grant 335262, and Grant 345072; in part by JSPS KAKENHI Grant Number 23K16877; and in part by the Project of Cyber Security Establishment with Inter-University Cooperation. An earlier version of this paper was presented in part at the IEEE International Conference on Communications (ICC) 2024. The associate editor coordinating the review of this article and approving it for publication was M. Wang. *(Corresponding author: Jia Liu.)*

Zhao Li, Chengyu Liu, Lijuan Zhang, and Zheng Yan are with the School of Cyber Engineering, Xidian University, Xi'an 710071, China.

Kang G. Shin is with the Department of Electrical Engineering and Computer Science, University of Michigan, Ann Arbor, MI 48019 USA.

Jia Liu is with the Center for Strategic Cyber Resilience Research and Development, National Institute of Informatics, Tokyo 101-8430, Japan (e-mail: jliu@nii.ac.jp).

Riku Jäntti is with the Department of Information and Communications Engineering, Aalto University, 02150 Espoo, Finland.

Color versions of one or more figures in this article are available at https://doi.org/10.1109/TWC.2024.3366229.

Digital Object Identifier 10.1109/TWC.2024.3366229

destructive components. Nevertheless, these two methods can only exploit partial interference, i.e., either the reflected [9] or the constructive interferences [10], leaving the direct and destructive disturbances unused. The authors of [11] proposed interference recycling (IRC), according to which the interfered Tx no longer sends the desired data but designs a recycling data and loads it to the recycling signal for transmission. The recycling signal interacts with the interference so that the interfered Rx can recover the desired data from the mixed signal [11]. This method uses both the information and the energy carried by the interference, but it still requires a portion of the desired Tx's power to construct the recycling signal. Moreover, when the spatial characteristics of the interference and the desired data deviate from each other significantly, it incurs a large recycling power overhead. Therefore, it is of great practical importance to devise low-cost IM methods.

Recently, a programmable meta-surface array consisting of passive reflective elements, namely an *intelligent reflecting surface* (IRS), has received increasing attention [12], [13]. As one of the key technologies for 6G, IRS offers several advantages. First, IRS allows for the retention of the original wireless communication system's hardware architecture without requiring additional active radio frequency (RF) devices, hence minimizing the power consumption and hardware deployment costs [14]. Second, the IRS is controlled by the IRS controller connected to the Tx, and the phase and/or amplitude coefficients of the reflective elements can be flexibly adjusted with software; this enables the control of the phase and intensity of the reflected signals, improving data transmission [15], [16], enhancing communication security [15], [17], [18], [19], and achieving interference management [14], [20]. Moreover, IRS can even be used for reconfiguration and detection of the wireless channel environment [15], [21]. However, the current limited research on IRS-based IM still treats interference as harmful. How to fully leverage interference with IRS to achieve efficient data transmission remains unexplored.

Furthermore, while there have been numerous studies on IRS, most of them simply use the conventional signal transmission model for method design and performance evaluation. However, this approach can "double-count" signal power, as the incident signal to the IRS is only a part of the original signal from the source. Consequently, this can mislead IRS-based method design and result in inaccurate performance evaluation. Therefore, we need to develop a more accurate and practical signal transmission model suitable for IRS investigation.

Based on the above discussion, we utilize the theory of power radiation pattern (PRP) [22] to modify the conventional signal transmission model, and then employ IRS to effectively manage interference and achieve efficient data transmission.

The contributions of this paper are three-fold:

- Development of a modified signal transmission model suitable for IRS-based method design and evaluation. By incorporating the PRP of transmit/receive antennas and IRS elements, a more realistic and accurate model is achieved.
- Proposal of *Intelligent Reflecting Surface Assisted Interference Exploitation (IRS-IE)*. We use the IRS to reflect the interference to the interfered Rx, so that the reflected component can interact with the direct counterpart, allowing the interfered Rx to recover the desired data from the mixed interference. This way, IRS-IE enables the efficient utilization of the energy and data information carried by the interference, thereby realizing low-cost IM to facilitate the desired transmission.
- Extended design of IRS-IE to more general situations. First, we allow the PBS to send a recycling signal, which can enhance the feasibility of IRS-IE and improve the quality of desired transmission. Second, we investigate the application of IRS-IE under more general modulation schemes.

The rest of this paper is organized as follows. Section II provides an overview of related works while Section III describes the system model. Section IV presents the design of IRS-IE. Section V explores the extended design of IRS-IE, and Section VI evaluates the performance of the proposed method via simulation. Finally, we conclude this paper in Section VII.

Throughout this paper, we will use the following notations. $\mathbb{C}$ represents the set of complex numbers. Scalars are represented by non-bold italic letters, while vectors and matrices are represented by lower- and upper-case bold letters, respectively. $\boldsymbol{X}^H$ denotes the Hermitian of matrix $\boldsymbol{X}$. $|x|$ indicates the absolute value of x.

II. Related Work

Among the IM methods mentioned in Section I, SIC [2], [3], [4] lets the Rx detect the information carried by a signal component from the received mixed signal in a sequential manner. Upon detection of a signal component, it is reconstructed based on the detected data and then subtracted from the mixed signal. This process continues until all signal components are detected. ZFBF [5] designs the precoding of the interference source to create multiple interferences that are orthogonal to the desired signal at the interfered Rx. This way, ZFBF can prevent interferences from affecting the desired transmission. IA [6] employs transmit precoding to restrict multiple interference components to a subspace of finite dimension at the interfered Rx. This allows the desired signal to be transmitted through an interference-free signal subspace. The authors of [23] have demonstrated the feasibility of IA to be highly dependent on the parameter settings of the communication system, including the numbers of Txs and Rxs, the numbers of transmit and receive antennas, etc. However, further research has revealed that interference can be not only aligned but also completely or partially eliminated by exploiting the signal propagation of multiple paths, which is known as interference neutralization (IN) [7], [24], [25]. IN eliminates interference by combining interferences from different paths in a destructive manner, while preserving the desired signal [24]. Essentially, IN exploits the interactions between wireless signals/interferences to cancel out the multiple interferences arriving from the interfering source at the interfered Rx [25]. However, none of the above-mentioned IM methods are cost-free. Specifically, they either sacrifice some desired signal's transmission quality or consume communication resources, such as transmit power and spatial DoFs. Most importantly, they treat interference as a negative factor and aim to eliminate its impact on the desired signal transmission. In contrast, the proposed IRS-IE collects the scattered energy from the interfering source and utilizes it to realize the desired data transmission.

As for the IRS-related works, [14] applied IRS to manage inter-cell interference in cellular systems. By designing the reflection coefficient of IRS, the desired signal components are constructively superimposed at the intended Rx while the interferences from the neighboring cells are canceled via destructive combination. The authors of [15] leveraged the potential of IRS to reconfigure the propagation environments and employed IRS to enhance the performance of unmanned aerial vehicle (UAV)-aided air-ground networks. By jointly optimizing the UAV trajectory, they were able to enhance the average achievable rate of the IRS-assisted relaying network and effectively thwart adversarial eavesdropping attempts. IRS was adopted in [16] to assist UAV in achieving energy-efficient transmission. Specifically, the energy-efficiency was maximized by jointly optimizing the UAV trajectory, transmit power, and IRS phase shifts based on the statistical CSI. The authors of [17] proposed a deep learning approach to jointly optimize the BS's power allocation and IRS's reflection beamforming to counteract malicious jammers located near multiple legitimate mobile users and send fake jamming signals through multiple antennas. Then, without the need for interference model information, system spectral efficiency can be maximized. The authors of [18] proposed a joint optimization of aerial IRS (AIRS) deployment and passive beamforming to mitigate jamming attacks and enhance legitimate transmission. The position of AIRS is determined via successive convex approximation, while the reflection beamforming is obtained using manifold optimization. IRS was integrated with UAV in [19] to enhance security in wireless networks. Through the joint optimization of UAV trajectory, transmit beamforming, and phase shifts of the IRS, the average secrecy rate of IRS-assisted UAV wireless networks was maximized. The authors of [20] studied the interference cancellation ability of IRS in a multi-user environment, where multiple single-antenna transceivers communicate simultaneously in a shared spectrum. They proposed a method to maximize the actual sum rate while taking into account interference-nulling constraints. The method uses the zero-forcing solution obtained from alternating projection as an initial point for subsequent Riemannian conjugate gradient optimization. Additionally, the authors introduced a subgradient projection method with low computational complexity to maximize the minimum sum rate. In [21], an IRS is used to facilitate non-line-of-sight (NLoS) communication where obstacles obstruct the direct transmission path between BS and mobile users. By reflecting the desired signal, the IRS creates a virtual line-of-sight (LoS) link that circumvents the obstacles and effectively targets the desired Rx. This approach helps eliminate signal coverage dead zones and enhances communication performance. In summary, IRS has the potential to facilitate the design of cost-effective IM methods due to its low power consumption, flexible deployment, and controllable signal adjustment capabilities. Based on the above review, existing IRS-related designs mainly focus on transmission enhancement, physical-layer security, and interference mitigation. However, to the best of our knowledge, none of them attempt to leverage IRS for interference exploitation. In contrast, the proposed IRS-IE utilizes IRS to collect and reflect the interference, thereby enabling its exploitation.

As is commonly known, it is crucial to establish an appropriate channel model for accurate evaluation of IRS utilization [26]. Some researchers emphasize practical channel modeling for IRS-empowered systems. For example, [26] explored potential use cases for IRS in future wireless systems while accounting for various indoor and outdoor wireless propagation environments as well as practical 5G channel model issues, and proposed a new software tool for IRS-empowered millimeter-wave communication systems. The authors of [27] proposed a hybrid far- and near-field stochastic channel model for characterizing an IRS-assisted vehicle-to-vehicle propagation environment. To reduce modeling complexity, they developed a sub-array partitioning scheme to dynamically divide the entire IRS array into several smaller sub-arrays, enabling the application of the planar wavefront assumption to these sub-arrays. On the other hand, numerous other researchers focus on designing IRS-assisted transmission mechanisms with commonly used classical wireless channel models, such as Rayleigh to characterize the IRS links. Unfortunately, this simplified application of channel models tends to overlook the distinct features of the reflecting and direct links, potentially misleading the design of IRS-based methods and incurring inaccurate performance evaluation. Specifically, these studies primarily rely on the conventional signal transmission model. In this model, the power collected by each IRS element is calculated based on the Tx's power. Consequently, as the number of IRS elements increases, the power of the reflected signal from the IRS also increases. This results in double-counting the Tx's power. Clearly, such a simplistic utilization of the conventional transmission model is inaccurate because, in practice, the power captured by the IRS is only a fraction of the transmission power used by the Tx. To address this problem, we will incorporate the theory of PRP [22] to modify the conventional signal transmission model. Then, we can develop a more realistic and accurate model suitable for the design and evaluation of IRS-based methods.

III. System Model

A. Basic System Assumptions

We consider downlink communication in heterogeneous cellular networks (HCNs) with overlapping macro base station (MBS) and pico base station (PBS), as shown in Fig. 1. The MBS controls an IRS consisting of $M > 1$ reflective elements. MBS and PBS are equipped with $N_{T_1} \geq 1$ and $N_{T_0} \geq 1$ transmit antennas, macro user equipment (MUE) and pico user equipment (PUE) are equipped with $N_{R_1} \geq 1$ and $N_{R_0} \geq 1$ receive antennas, respectively. We use P_{T_1} and P_{T_0} to denote the transmit power of MBS and PBS. MBS transmits a signal carrying data x_1 to MUE and causes interference to

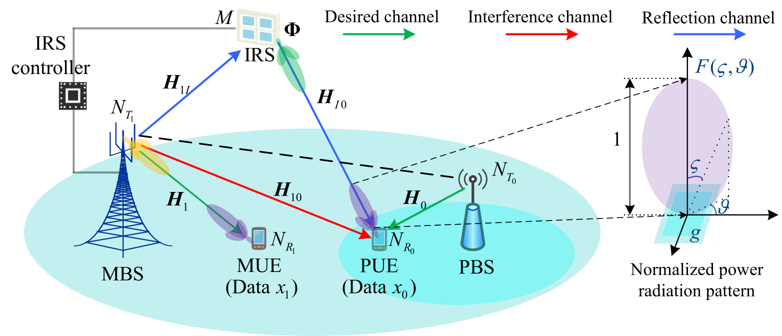

Fig. 1. System model.

PUE. x_0 denotes the desired data that PBS intends to send to PUE. In our system model, we assume the interference from PBS to MUE is negligible.[1] We use $\boldsymbol{H}_0 \in \mathbb{C}^{N_{R_0}\times N_{T_0}}$, $\boldsymbol{H}_1 \in \mathbb{C}^{N_{R_1}\times N_{T_1}}$, $\boldsymbol{H}_{10} \in \mathbb{C}^{N_{R_0}\times N_{T_1}}$, $\boldsymbol{H}_{1I} \in \mathbb{C}^{M\times N_{T_1}}$, and $\boldsymbol{H}_{I0} \in \mathbb{C}^{N_{R_0}\times M}$ to represent the channel matrices from PBS to PUE, MBS to MUE, MBS to PUE, MBS to IRS, and IRS to PUE, respectively. Because IRS is controlled by the MBS, MBS can accurately estimate $\boldsymbol{H}_{1I}$. In addition, MUE can estimate $\boldsymbol{H}_1$, and PUE can measure $\boldsymbol{H}_0$, $\boldsymbol{H}_{10}$, and $\boldsymbol{H}_{I0}$. Both MUE and PUE feed the above channel matrices (a.k.a. channel state information (CSI)) to their respective BS through a low-rate error-free link, and the transmission delay can be ignored compared to the time scale of the channel state change [29]. Since MBS and PBS are usually deployed by the same operator [11], we can assume that PBS can share PUE's CSI and desired data information (i.e., x_0) with MBS via inter-BS collaboration.

IRS connects to MBS through the IRS controller. IRS controller coordinates the CSI collection and signaling transmission between MBS and IRS [30], [31]. Each element of IRS independently adjusts the incident signal's phase and amplitude and reflects it to PUE. IRS's reflection coefficient matrix is expressed by an $M \times M$ complex matrix $\boldsymbol{\Phi} = diag(\gamma_1, \cdots, \gamma_i, \cdots, \gamma_M)$, where $diag(\cdot)$ represents for the diagonalization of a vector. $\gamma_i = \psi_i e^{j\theta_i}$ denotes the reflection coefficient of the i^{th} element where $i \in \{1, 2, \cdots, M\}$. $\psi_i \in [0, 1]$[2] and $\theta_i \in [-\pi, \pi)$ are the amplitude coefficient and phase shift coefficient, respectively. For simplicity, we ignore the signal component that is reflected twice or more [30].

In practice, we can employ a high-speed control link to facilitate both the delivery of phase-shift information from the MBS to IRS and data sharing from the PBS to MBS. Thus, the IRS controller can adjust the reflection coefficient of each IRS element in real time [9]. In existing communication systems, such as coordinate multi-point (CoMP) and HCNs, researchers have reached a consensus that low-latency and high-capacity wired/wireless backhaul (i.e., control or signaling) link can be established among communication entities [32], [33], [34].

In our system model, we omit the reflected signal from MBS to the MUE via IRS. This is because, in practice, to improve the received signal's quality, the main lobe of the PRP of the MBS's transmit antenna and that of the MUE's receive antenna should be aligned with each other (a detailed discussion of PRP can be found in Section III-B). Similarly, as the IRS is designed to reflect the signal from MBS to PUE, the PRP of the IRS elements should align with that of the PUE's antenna. Therefore, the signal from MBS via IRS to MUE is negligible. Additionally, note that the reflected signal originating from MBS is the desired signal for MUE, and in our system, we deploy the IRS in close proximity to the MBS, allowing both the direct and reflected desired signals to arrive at the MUE synchronously. Then, regardless of whether the desired reflected signal happens to enhance or weaken its direct counterpart at the MUE, considering the reflected component is relatively small, its impact on the MUE's reception can be deemed negligible.

Before delving into details, we provide the main parameters used in this paper in Table I.

B. A Modified Signal Transmission Model

The power radiation pattern (PRP) shown in the subgraph of Fig. 1 illustrates the variation of the power radiated or received by an antenna, providing a visual representation of the direction from which the antenna transmits or receives the maximum power. The PRP is determined by the hardware properties of the antenna [22]. In this section, we will leverage the theory of PRP to derive a modified signal transmission model that is appropriate for IRS-based method design.

In practice, to improve the received signal's quality, the main lobe of the PRP of the transmit antenna and that of the receive antenna should be aligned with each other. Moreover,

[1]The power of MBS is known to be several to even hundreds of times greater than the power of PBS [28]. Moreover, picocells are typically deployed at the edge of a macrocell to enhance signal coverage or facilitate traffic offloading. Consequently, the MUE can receive a much stronger desired signal than the interference from the PBS. Furthermore, when the PBS transmits to its intended PUE, in order to improve the received signal's quality, the main lobes of the PRP of the transmit antenna and its intended receive antenna should be aligned with each other. As a result, the interference power leaked to the MUE is limited. Therefore, the disturbance from PBS to MUE is omitted in Fig. 1. In addition, since the IRS is configured to reflect signal to the PUE, its PRP is directed towards the PUE. Simultaneously, considering the transmission distance and path loss between the PBS and the IRS, the interference from PBS to MUE via IRS is significantly smaller than the direct interference from PBS to MUE, thus making it negligible.

[2]Existing research categorizes IRS into two types: passive IRS and active IRS. In this paper, we present the IRS-IE under the constraint that the amplitude coefficient of the IRS should be confined within the range $[0, 1]$ for low power cost. Additionally, in the discussion of Fig. 2, we conclude that under MPSK, the amplitude coefficient of the IRS should be set to 1 in order to achieve the best reception performance possible. These characteristics align with the nature of passive IRS, so the IRS utilized in our work falls into the passive category.

TABLE I
TABLE OF PARAMETERS

Parameter	Description
P_{T_0}, P_{T_1}	Transmit power of PBS and MBS
N_{T_0}, N_{T_1}	The numbers of PBS and MBS's antennas
N_{R_0}, N_{R_1}	The numbers of PUE and MUE's antennas
x_0, x_1	Desired data of PBS and MBS
$\boldsymbol{H}_1$	Channel matrices between MBS and MUE
$\boldsymbol{H}_{10}$, $\boldsymbol{H}_{1I}$	Channel matrices between MBS and PUE/IRS
$\boldsymbol{H}_0$, $\boldsymbol{H}_{I0}$	Channel matrices between PBS/IRS and PUE
M	The number of IRS elements
$\boldsymbol{\Phi}$	Reflection coefficient matrix of IRS
γ_i	Reflection coefficient of the i^{th} IRS element
ψ_i, θ_i	Amplitude/Phase-shift coeffs. of the i^{th} IRS element
$F(\cdot)$	The normalized PRP
ς, ϑ	Elevation and azimuth angles between antennas
$F^a(\cdot)$	The normalized PRP of equipment a's antenna/element
$F_b^a(\cdot)$	Value of $F^a(\cdot)$ in the direction of equipment b
ζ	Pct. of MBS power collected by MUE, PUE, and IRS
$M_{\max}$	The maximum number of IRS elements
$\bar{x}_0$	Data recovered by PUE
λ	A real scaling factor for x_0 resulting in $\bar{x}_0$
s_1	Direct interference
$s_I^{(i)}$	The i^{th} reflected interference component
s_I	The sum of M reflected interference components
φ_1, $\varphi_I^{(i)}$, φ_I	The phases of s_1, $s_I^{(i)}$, and s_I
ρ_1, $\rho_I^{(i)}$, ρ_I	The modulus of s_1, $s_I^{(i)}$, and s_I
$\tilde{s}_I^{(i)}$, $\tilde{\varphi}_I^{(i)}$	$s_I^{(i)}/\gamma_i$ and its phase
κ_0, κ_1	Amplitudes of x_0 and x_1
ϕ_0, ϕ_1	Phases of x_0 and x_1
ω_1, ω_2	Angles between two vectors
φ_δ	Phase difference between s_1 and x_0
$\boldsymbol{h}_{1I}^{(i)}$, $\boldsymbol{h}_{I0}^{(i)}$	The i^{th} row and column of $\boldsymbol{H}_{1I}$ and $\boldsymbol{H}_{I0}$
$\boldsymbol{z}_0$, σ_n^2	AWGN vector and its element's power
α	Power utility factor of the direct interference perceived by PUE from MBS
η	Power utility factor of the reflected signal received by PUE from IRS element
P_{t_0}	Effective power of PBS radiating to PUE
P_{t_1}, $\tilde{P}_{t_1}$	Effective power of MBS radiating to MUE and PUE
s_{RS}	Recycling signal received by PUE from PBS
ρ_{RS}, ϕ_{RS}	Amplitude and phase of s_{RS}
$\boldsymbol{p}_{RS}$	Precoding vector for s_{RS} at the PBS
$\boldsymbol{p}_0$, $\boldsymbol{p}_1$	Precoding vectors for x_0 and x_1 at PBS and MBS
$\boldsymbol{f}_0$, $\boldsymbol{f}_1$	Filter vectors at PUE and MUE
ε	The normalized value of MBS's power to noise
$\boldsymbol{y_0}$	The mixed signal received by PUE
$\hat{y}_0$	The estimated signal at PUE
τ	The ratio of P_{T_0} to P_{T_1}

based on the definition of PRP, the radiation power from the MBS to the MUE/PUE is jointly determined by the PRP of the antennas/elements of MBS, IRS, and MUE/PUE. In the proposed IRS-IE, as depicted in Fig. 1, we assume that PBS does not send any signal — in this case, the lower bound of the data rate for PUE can be obtained. However, in practice, PBS can transmit signals to further enhance the pico transmission performance. Thus, we align the main lobes of the MBS and MUE, as well as the IRS and PUE, with each other, respectively. In what follows, we will derive the expressions of the radiated/received power of MBS, MUE, IRS, and PUE, respectively, in the scenario of HCNs, as illustrated in Fig. 1.

For clarity, we define the power radiation intensity in the central direction of the main lobe as 1. Then, we can express the normalized PRP as a function $F(\varsigma,\vartheta)$ in the spherical coordinate system where ς and ϑ denote the elevation and azimuth angles, respectively, from antenna g to a particular transmit or receive antenna. By substituting parameters ς and ϑ into $F(\varsigma,\vartheta)$, we can calculate the power radiation intensity of antenna g in the direction specified by ς and ϑ. When the distance between the Tx and the receive antenna array is large enough, the spherical wave generated by the transmit antenna array can be approximated as a plane wave upon reaching the receive antenna array. As a result, the radiation pattern of the transmit (or receive) antenna array is only affected by the elevation angle of the receive (or transmit) antenna with respect to (w.r.t.) the direction of the Tx (or Rx). Thus, based on the assumption of plane wave, the expression of $F(\varsigma,\vartheta)$ is given as [22]:

$$F(\varsigma,\vartheta)=\begin{cases}\cos^3\varsigma, & \varsigma\in[0,\pi/2],\ \vartheta\in(0,2\pi]\\ 0, & \varsigma\in(\pi/2,\pi],\ \vartheta\in(0,2\pi]\end{cases}. \qquad (1)$$

From Eq. (1) and the right subfigure of Fig. 1, we can find that $F(\varsigma,\vartheta)$ only depends on the elevation angle ς. Moreover, $F(\varsigma,\vartheta)$ reaches its maximum when $\varsigma=0$, indicating that antenna g has the maximum power radiation intensity in the direction defined by $\varsigma=0$.

We use $F^{tM}(\varsigma^{tM},\vartheta^{tM})$, $F^{I}(\varsigma^{I},\vartheta^{I})$, $F^{rM}(\varsigma^{rM},\vartheta^{rM})$, and $F^{rP}(\varsigma^{rP},\vartheta^{rP})$ to represent the normalized PRP of the MBS's transmit antenna, IRS's element (assuming all IRS elements have the same radiation characteristics), MUE's receive antenna, and PUE's receive antenna, respectively. Note that $F^{I}(\varsigma^{I},\vartheta^{I})$ takes into account the relationship between the incident power radiation intensity and the incident angle, as well as the reflected power radiation intensity and reflected angle of the IRS element. We employ a general formula $F_b^a(\varsigma_b^a,\vartheta_b^a)$ to represent the value of the radiation direction function $F^a(\varsigma^a,\vartheta^a)$ for equipment a in the direction of equipment b determined by the elevation angle ς_b^a and azimuth angle ϑ_b^a. It represents the normalized power radiation intensity, where $a\in\{tM,I,rM,rP\}$ and $b\in\{tM,I,rM,rP\}$. Here, tM, I, rM, and rP stand for MBS, IRS, MUE, and PUE, respectively. For instance, $F_{rM}^{tM}(\varsigma_{rM}^{tM},\vartheta_{rM}^{tM})$ represents the power radiation intensity of the MBS's radiation direction function $F^{tM}(\varsigma^{tM},\vartheta^{tM})$ in the direction of MUE.

Based on the derivation of the Rx's received power expression in [22] under the far-field beam condition, we can express the received power of the MUE as being proportional to $F_{rM}^{tM}(\varsigma_{rM}^{tM},\vartheta_{rM}^{tM})$ and $F_{tM}^{rM}(\varsigma_{tM}^{rM},\vartheta_{tM}^{rM})$, and the received power of the PUE as being proportional to $F_{I}^{tM}(\varsigma_{I}^{tM},\vartheta_{I}^{tM})$, $F_{tM}^{I}(\varsigma_{tM}^{I},\vartheta_{tM}^{I})$, $F_{rP}^{I}(\varsigma_{rP}^{I},\vartheta_{rP}^{I})$, and $F_{I}^{rP}(\varsigma_{I}^{rP},\vartheta_{I}^{rP})$. Therefore, the function values of $F^{tM}(\varsigma^{tM},\vartheta^{tM})$ in the direction of MUE, PUE, and IRS are $F_{rM}^{tM}(\varsigma_{rM}^{tM},\vartheta_{rM}^{tM})=1$, $F_{rP}^{tM}(\varsigma_{rP}^{tM},\vartheta_{rP}^{tM})$, and $F_{I}^{tM}(\varsigma_{I}^{tM},\vartheta_{I}^{tM})$, respectively, which satisfy $F_{rM}^{tM}(\varsigma_{rM}^{tM},\vartheta_{rM}^{tM}) > F_{rP}^{tM}(\varsigma_{rP}^{tM},\vartheta_{rP}^{tM})$ and $F_{rM}^{tM}(\varsigma_{rM}^{tM},\vartheta_{rM}^{tM}) > F_{I}^{tM}(\varsigma_{I}^{tM},\vartheta_{I}^{tM})$. The function values of $F^{I}(\varsigma^{I},\vartheta^{I})$ in the direction of PUE, MUE, and MBS are $F_{rP}^{I}(\varsigma_{rP}^{I},\vartheta_{rP}^{I})=1$, $F_{rM}^{I}(\varsigma_{rM}^{I},\vartheta_{rM}^{I})$, and $F_{tM}^{I}(\varsigma_{tM}^{I},\vartheta_{tM}^{I})$, respectively, satisfying $F_{rP}^{I}(\varsigma_{rP}^{I},\vartheta_{rP}^{I}) > F_{rM}^{I}(\varsigma_{rM}^{I},\vartheta_{rM}^{I})$ and $F_{rP}^{I}(\varsigma_{rP}^{I},\vartheta_{rP}^{I}) > F_{tM}^{I}(\varsigma_{tM}^{I},\vartheta_{tM}^{I})$. The function values of $F^{rM}(\varsigma^{rM},\vartheta^{rM})$ in the direction of MBS and IRS are $F_{tM}^{rM}(\varsigma_{tM}^{rM},\vartheta_{tM}^{rM})=1$ and $F_{I}^{rM}(\varsigma_{I}^{rM},\vartheta_{I}^{rM})$, respectively, which satisfy $F_{tM}^{rM}(\varsigma_{tM}^{rM}, \vartheta_{tM}^{rM}) > F_{I}^{rM}(\varsigma_{I}^{rM}, \vartheta_{I}^{rM})$. The function values of $F^{rP}(\varsigma^{rP}, \vartheta^{rP})$ in the direction of IRS and MBS are $F_{I}^{rP}(\varsigma_{I}^{rP}, \vartheta_{I}^{rP}) = 1$ and $F_{tM}^{rP}(\varsigma_{tM}^{rP}, \vartheta_{tM}^{rP})$, respectively, satisfying $F_{I}^{rP}(\varsigma_{I}^{rP}, \vartheta_{I}^{rP}) > F_{tM}^{rP}(\varsigma_{tM}^{rP}, \vartheta_{tM}^{rP})$.

In summary, we use P_{t_1} to denote the effective power radiated by the MBS to MUE, and we use $\tilde{P}_{t_1}$ to denote the effective power (interference) radiated by the MBS to PUE, where $\tilde{P}_{t_1} = \alpha P_{t_1}$ and α is the power utility factor of direct interference w.r.t. the PUE. Specifically, we have $\alpha = F_{rP}^{tM}(\varsigma_{rP}^{tM}, \vartheta_{rP}^{tM}) F_{tM}^{rP}(\varsigma_{tM}^{rP}, \vartheta_{tM}^{rP})$. Since MBS radiates most power to MUE and there is a distance between PUE and MUE, the direct interference experienced by the PUE only accounts for a small portion of the total radiated power from the MBS. Therefore, we take α as a few tenths. The effective power of PBS radiating to PUE is denoted as P_{t_0}, which satisfies $P_{t_1} < P_{T_1}$, $\tilde{P}_{t_1} < P_{T_1}$, and $P_{t_0} < P_{T_0}$. As reported in [28], P_{T_1} is typically several times or even hundreds of times greater than P_{T_0}, resulting in a significant direct interference from MBS to PUE that needs to be managed. Moreover, the reflected interference from the IRS to PUE is also strong enough to be utilized in mitigating the direct interference from the MBS [35]. However, it's important to note that we will exploit the reflected interference to interact with its direct counterpart, outputting a signal that carries the desired data for the PUE. The IRS reflects the radiated power from MBS to PUE. The effective power of the reflected signal received by the PUE from the i^{th} IRS element is denoted as $\eta_i P_{t_1}$, where η_i is the power utility factor of the reflected signal received by the PUE from the i^{th} IRS element. The value of η_i is primarily determined by the PRP of MBS, PUE, and IRS, as well as the relative position of IRS w.r.t. MBS and PUE antennas [22]. In the far-field case, where all η_i ($i \in \{1, 2, \cdots, M\}$) have the same value, we can simplify the notation by using η to represent η_i, and obtain $\eta = F_{I}^{tM}(\varsigma_{I}^{tM}, \vartheta_{I}^{tM}) F_{tM}^{I}(\varsigma_{tM}^{I}, \vartheta_{tM}^{I}) F_{rP}^{I}(\varsigma_{rP}^{I}, \vartheta_{rP}^{I}) F_{I}^{rP}(\varsigma_{I}^{rP}, \vartheta_{I}^{rP})$. Since $F_{I}^{rP}(\varsigma_{I}^{rP}, \vartheta_{I}^{rP}) = 1$ and $F_{rP}^{I}(\varsigma_{rP}^{I}, \vartheta_{rP}^{I}) = 1$, we have $\eta = F_{I}^{tM}(\varsigma_{I}^{tM}, \vartheta_{I}^{tM}) F_{tM}^{I}(\varsigma_{tM}^{I}, \vartheta_{tM}^{I})$. As a result, η has a value that is a few hundredths.

Note that except for the power that MBS radiates to MUE and PUE, there is still some power that is emitted into the open space. The IRS can capture a portion, but not all, of the remaining power radiated from the MBS. According to the energy conservation law, we have $P_{t_1} + \tilde{P}_{t_1} + \sum_{i=1}^{M} \eta P_{t_1} \leq \zeta P_{T_1}$ where $\sum_{i=1}^{M} \eta P_{t_1}$ is the power that PUE receives from IRS's M elements. Assuming that MUE, PUE, and IRS can gather the majority of MBS's radiated power, we let ζ approach 1. Then, we can easily see from the above inequality that as the number of IRS elements increases to a certain value, say $M_{\max}$, $P_{t_1} + \tilde{P}_{t_1} + \sum_{i=1}^{M} \eta P_{t_1}$ will approach ζP_{T_1}, which is upper-bounded by P_{T_1}. In other words, the continuous increase of M will not cause the power collected by the IRS to increase without limit. Based on the above discussion, we let $M \leq M_{\max}$; when $M = M_{\max}$, $P_{t_1} + \tilde{P}_{t_1} + \sum_{i=1}^{M} \eta P_{t_1} = \zeta P_{T_1}$ holds. As for the MUE, we disregard the reflected desired signal that is transmitted from MBS to it via IRS. Moreover, as MUE is outside the PBS's communication range, the interference power reaching MUE from the PBS or from the PBS via IRS is significantly lower than the desired signal's power radiated from MBS. Therefore, the interference experienced by the MUE is considered negligible. Therefore, in the design of IRS-IE we focus on improving the transmission efficiency for the PUE.

IV. Design of IRS-IE

We now present the design of IRS-IE with MBS employing M-ary Phase Shift Keying (MPSK) modulation, and MUE and PUE accordingly adopting MPSK demodulation, as an example.

Since we assume PBS does not send any signal, the mixed signal received by PUE can be expressed as:

$$\boldsymbol{y}_0 = \sqrt{\alpha P_{t_1}} \boldsymbol{H}_{10} \boldsymbol{p}_1 x_1 + \sqrt{\eta P_{t_1}} \boldsymbol{H}_{I0} \boldsymbol{\Phi} \boldsymbol{H}_{1I} \boldsymbol{p}_1 x_1 + \boldsymbol{z}_0, \quad (2)$$

where the first term on the right-hand side (RHS) of Eq. (2) denotes the direct interference from MBS, while the second term is the reflected interference reaching PUE via IRS. $\boldsymbol{z}_0$ represents for the additive white Gaussian noise (AWGN) vector whose elements have zero-mean and variance σ_n^2. $\boldsymbol{p}_1$ is the precoding vector at the MBS. The i^{th} column of $\boldsymbol{H}_{I0}$ and the i^{th} row of $\boldsymbol{H}_{1I}$ are denoted by $\boldsymbol{h}_{I0}^{(i)}$ and $\boldsymbol{h}_{1I}^{(i)}$, respectively, where $i \in \{1, 2, \cdots, M\}$. Then, Eq. (2) can be rewritten as:

$$\boldsymbol{y}_0 = \sqrt{\alpha P_{t_1}} \boldsymbol{H}_{10} \boldsymbol{p}_1 x_1 + \sqrt{\eta P_{t_1}} \sum_{i=1}^{M} \boldsymbol{h}_{I0}^{(i)} \psi_i e^{j\theta_i} \boldsymbol{h}_{1I}^{(i)} \boldsymbol{p}_1 x_1 + \boldsymbol{z}_0. \quad (3)$$

We employ a unit vector $\boldsymbol{f}_0 \in \mathbb{C}^{N_{R_0} \times 1}$ as the receive filter at the PBS. Then, the estimated signal can be obtained as:

$$\hat{y}_0 = \sqrt{\alpha P_{t_1}} \boldsymbol{f}_0^H \boldsymbol{H}_{10} \boldsymbol{p}_1 x_1 + \sqrt{\eta P_{t_1}} \sum_{i=1}^{M} \boldsymbol{f}_0^H \boldsymbol{h}_{I0}^{(i)} \psi_i e^{j\theta_i} \boldsymbol{h}_{1I}^{(i)} \boldsymbol{p}_1 x_1 + \boldsymbol{f}_0^H \boldsymbol{z}_0. \quad (4)$$

Note that $\boldsymbol{f}_0^H \boldsymbol{H}_{10} \boldsymbol{p}_1$, $\boldsymbol{f}_0^H \boldsymbol{h}_{I0}^{(i)} \psi_i e^{j\theta_i} \boldsymbol{h}_{1I}^{(i)} \boldsymbol{p}_1$, and $\boldsymbol{f}_0^H \boldsymbol{z}_0$ are complex coefficients. To recover the desired data x_0, the RHS of Eq. (4) should satisfy:

$$\sqrt{\alpha P_{t_1}} \boldsymbol{f}_0^H \boldsymbol{H}_{10} \boldsymbol{p}_1 x_1 + \sqrt{\eta P_{t_1}} \sum_{i=1}^{M} \boldsymbol{f}_0^H \boldsymbol{h}_{I0}^{(i)} \psi_i e^{j\theta_i} \boldsymbol{h}_{1I}^{(i)} \boldsymbol{p}_1 x_1 = \lambda x_0. \quad (5)$$

From Eq. (5), we can see that the estimated data of PUE extracted from the post-processed mixed signal may be its desired data x_0 scaled by a factor λ. We define $\bar{x}_0 = \lambda x_0$ where λ is a real number. $\bar{x}_0$ can be either in-phase with (i.e., $\lambda > 0$) or in the opposite phase with (i.e., $\lambda < 0$) x_0. The polarity of λ can be fed to PUE via an error-free low-rate link.

The unknown variables on the left-hand side (LHS) of Eq. (5) are ψ_i and θ_i ($i \in \{1, 2, \cdots, M\}$), both determine the reflection coefficient $\psi_i e^{j\theta_i}$ of the i^{th} IRS element. IRS-IE needs to design each $\psi_i e^{j\theta_i}$ so that PUE can recover its desired data from the received mixed interference. In Eq. (5), the variables (i.e., amplitude and phase) of the first term on the LHS are known. For clarity, we define it as $\sqrt{\alpha P_{t_1}} \boldsymbol{f}_0^H \boldsymbol{H}_{10} \boldsymbol{p}_1 x_1 = s_1$. The second term on the LHS of Eq. (5) is the sum of the M reflected interference components, which we define as s_I. Note that in s_I, all variables except for ψ_i and θ_i are known, so we define the i^{th} component and its amplitude and phase as $s_I^{(i)}$, $\rho_I^{(i)} > 0$, and $\varphi_I^{(i)} \in (-\pi, \pi]$, respectively. $\rho_I^{(i)}$ is affected by ψ_i ($\psi_i \in [0, 1]$), while $\varphi_I^{(i)}$ is

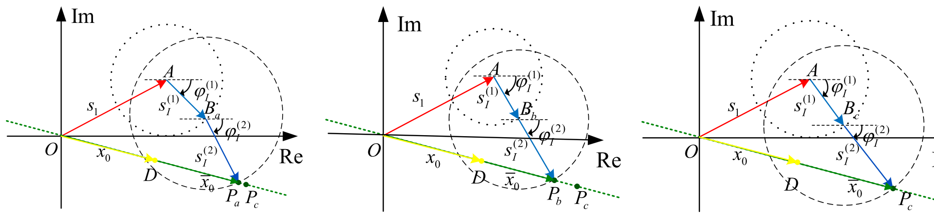

(a) Non-aligned $s_I^{(i)}$ and $\psi_i = 1$. (b) Aligned $s_I^{(i)}$ and $\psi_i < 1$. (c) Aligned $s_I^{(i)}$ and $\psi_i = 1$.

Fig. 2. Illustration of the impact of ψ_i and θ_i on $|\lambda|$ under $M = 2$, and given s_1 and x_0.

influenced by θ_i ($\theta_i \in (-\pi, \pi]$). Therefore, we can have $s_I^{(i)} = \sqrt{\eta P_{t_1}} \boldsymbol{f}_0^H \boldsymbol{h}_{I0}^{(i)} \boldsymbol{h}_{1I}^{(i)} \boldsymbol{p}_1 x_1 \cdot \psi_i e^{j\theta_i} = \rho_I^{(i)} e^{j\varphi_I^{(i)}}$. λ on the RHS of Eq. (5) is influenced jointly by ψ_i and θ_i. By properly setting ψ_i and θ_i, one can achieve λ as a real number with the largest possible magnitude, denoted as $|\lambda|$. This enables the PUE to recover its desired data with the highest quality. In what follows, we will explore the impact of the values of ψ_i and θ_i on $|\lambda|$.

Fig. 2 illustrates the influence of ψ_i and θ_i on $|\lambda|$ under $M = 2$, and given s_1 and x_0. In the figure, we use vectors to represent s_1, $s_I^{(i)}$, and x_0 in the complex plane, where the length of the vector is the modulus of the complex number, while the angle between the vector and the positive real axis which is denoted by a directed arc represents the phase of the complex number. Note that the clockwise directed arc indicates that the phase ranges from 0 to $-\pi$, while the counterclockwise directed arc means the phase is in the range from 0 to π. We employ $\overrightarrow{OA}$, $\overrightarrow{OD}$, $\overrightarrow{AB_l}$, and $\overrightarrow{B_lP_l}$ (the subscript $l \in \{a, b, c\}$ indicates various subplot) to denote s_1, x_0, $s_I^{(1)}$, and $s_I^{(2)}$, respectively. For clarity, we draw two auxiliary circles, one with A as the center and $\rho_I^{(1)}$ (i.e., the modulus of $s_I^{(1)}$) as the radius, and the other with B_l as the center and $\rho_I^{(2)}$ (i.e., the modulus of $s_I^{(2)}$) as the radius. Recall that IRS-IE intends to enable PUE to recover its desired data from the mixed interference with the highest possible quality, the vector $\bar{x}_0$ (i.e., $\overrightarrow{OP_l}$) obtained by superimposing $s_I^{(1)}$, $s_I^{(2)}$, and s_1 should be in phase with x_0 (i.e., $\bar{x}_0 = \lambda x_0$ should hold. Note that in Fig. 2, we take $\lambda > 0$ as example, when $\lambda < 0$, the illustration is similar), and the length of $\overrightarrow{OP_l}$ (i.e., $|\lambda|$) should be maximized.

In Fig. 2(a), two reflected interference components have different phases at the PUE, i.e., $\varphi_I^{(1)} \neq \varphi_I^{(2)}$. When $\psi_i = 1$ ($i \in \{1, 2\}$), $\rho_I^{(1)}$ and $\rho_I^{(2)}$ are maximized. Vectors $s_I^{(1)}$ and $s_I^{(2)}$ superimpose with s_1 to output $\overrightarrow{OP_a}$. In Fig. 2(b), we use θ_i to let the reflected components at the PUE be in-phase, i.e., $\varphi_I^{(1)} = \varphi_I^{(2)}$ holds. However, we take $\psi_i < 1$, i.e., $\rho_I^{(1)}$ and $\rho_I^{(2)}$ are smaller than in Fig. 2(a). Then, in subfigure (b) vectors $s_I^{(1)}$ and $s_I^{(2)}$ interact with s_1 and yield $\overrightarrow{OP_b}$. In Fig. 2(c), we set θ_i to yield $\varphi_I^{(1)} = \varphi_I^{(2)}$ and let $\psi_i = 1$. Then, the reflected interference components can interact with s_1 to output $\overrightarrow{OP_c}$. For comparison, we have marked point P_c in both Figs. 2(a) and 2(b). One can see from subfigures (a) and (c) that $\overrightarrow{OP_c}$ is longer than $\overrightarrow{OP_a}$. This indicates that given same ψ_i, adjusting θ_i to let all of the reflected interferences be in-phase at the PUE allows the PUE to obtain $\bar{x}_0$ with a larger magnitude. Comparing Figs. 2(b) and 2(c), we can find that $\overrightarrow{OP_c}$ is longer than $\overrightarrow{OP_b}$. This means that for a set of determined θ_i, setting $\psi_i = 1$ enables PUE to recover its desired data better. In summary, to realize desired data recovery at the PUE, IRS-IE should set $\psi_i = 1$ and determine appropriate θ_i for each reflective element. This will allow the M reflected interference components to combine constructively (i.e., $\varphi_I^{(1)} = \cdots = \varphi_I^{(M)} = \varphi_I$ holds) and properly interact with the direct interference at the PUE.

Based on the above discussion, we substitute $\psi_i = 1$ into Eq. (5) and can get:

$$\sqrt{\alpha P_{t_1}} \boldsymbol{f}_0^H \boldsymbol{H}_{10} \boldsymbol{p}_1 x_1 + \sqrt{\eta P_{t_1}} \sum_{i=1}^{M} \boldsymbol{f}_0^H \boldsymbol{h}_{I0}^{(i)} \boldsymbol{h}_{1I}^{(i)} \boldsymbol{p}_1 x_1 \cdot e^{j\theta_i} \\ = \lambda x_0. \tag{6}$$

Since a data symbol can be represented by its amplitude and phase, we can define $x_0 = \kappa_0 e^{j\phi_0}$ and $x_1 = \kappa_1 e^{j\phi_1}$. So, the direct interference, the equivalent reflected interference, and the reflected interference component can be expressed in complex form as: $s_1 = \sqrt{\alpha P_{t_1}} \boldsymbol{f}_0^H \boldsymbol{H}_{10} \boldsymbol{p}_1 x_1 = \rho_1 e^{j\varphi_1}$, $s_I = \rho_I e^{j\varphi_I}$, and $s_I^{(i)} = \sqrt{\eta P_{t_1}} \boldsymbol{f}_0^H \boldsymbol{h}_{I0}^{(i)} \boldsymbol{h}_{1I}^{(i)} \boldsymbol{p}_1 x_1 \cdot e^{j\theta_i} = \rho_I^{(i)} e^{j\varphi^{(i)}}$. In the above expressions, the amplitudes κ_0, κ_1, ρ_I, ρ_1, and $\rho_I^{(i)}$ are positive real numbers, while the phases ϕ_0, ϕ_1, φ_I, φ_1, and $\varphi_I^{(i)}$ are in the range of $(-\pi, \pi]$. Then, Eq. (5) can be simplified as:

$$s_1 + \sum_{i=1}^{M} s_I^{(i)} = \lambda x_0. \tag{7}$$

According to the discussions of Fig. 2, when $\varphi_I^{(1)} = \cdots = \varphi_I^{(M)} = \varphi_I$ holds $s_I^{(i)}$ aligns with each other so that the amplitude of $\bar{x}_0$ is maximized. In this case, we can have:

$$\rho_I = \sum_{i=1}^{M} \rho_I^{(i)}. \tag{8}$$

Since only θ_i in $s_I^{(i)}$ is unknown, we define $\tilde{s}_I^{(i)} = \sqrt{\eta P_{t_1}} \boldsymbol{f}_0^H \boldsymbol{h}_{I0}^{(i)} \boldsymbol{h}_{1I}^{(i)} \boldsymbol{p}_1 x_1 = \rho_I^{(i)} e^{j\tilde{\varphi}_I^{(i)}}$ as the interference component without reflective phase shift. Then, we can get $\tilde{\varphi}_I^{(i)} = \varphi_I^{(i)} - \theta_i$ under the assumption that all of the phases and phase differences are in the range of $(-\pi, \pi]$. Furthermore, we can see that all variables in the expression of $\tilde{s}_I^{(i)}$ are known, so $\tilde{\varphi}_I^{(i)}$ is a known variable. Therefore, in order to compute θ_i to let $\varphi_I^{(1)} = \cdots = \varphi_I^{(M)} = \varphi_I$ hold, we need to calculate φ_I first, and then apply $\tilde{\varphi}_I^{(i)} = \varphi_I - \theta_i$ to determine θ_i. Based on the above analysis, we simplify Fig. 2(c) to Fig. 3 where the calculation of φ_I is illustrated.

As the figure shows, vectors $\overrightarrow{OA}$, $\overrightarrow{OD}$, and $\overrightarrow{AP}$ represent the direct interference s_1, desired data x_0, and the equivalent reflected interference s_I which is the combination of M in-phase reflected interference components $\tilde{s}_I^{(i)}$ ($i \in$

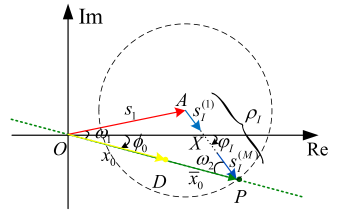

Fig. 3. Illustration of calculation of φ_I.

$\{1, \cdots, M\}$), respectively. The modulus of $\overrightarrow{AP}$ is ρ_I, while the superposition of s_1 and s_I results in $\overrightarrow{OP}$ (i.e., $\bar{x}_0$). In the figure, s_1, s_I, and $\bar{x}_0$ form a triangle $\triangle OAP$, which is divided by the real axis into two smaller triangles $\triangle OAX$ and $\triangle OXP$. We use directed arc to denote a vector's phase (e.g., φ_I) which is in the range of $(-\pi, \pi]$. Moreover, we employ an undirected arc to represent the angle between two vectors (e.g., ω_1 and ω_2), falling in the interval of $(0, \pi]$. Since x_0 (shared from PBS to MBS) and s_1 (MBS can get s_1 based on h_{10} and h_0 shared from PBS) are known, we can get the angle ω_1 between them. We denote the angle between x_0 and s_I as ω_2 which is to be determined. Then, to triangle $\triangle OXP$, we can apply the theorem "the exterior angle of a triangle is equal to the sum of its two non-adjacent interior angles" and get $\varphi_I = \phi_0 - \omega_2$ where ϕ_0 is the phase of x_0. To obtain φ_I, we need to calculate ω_2 according to the Sine rule as given by Eq. (9) below:

$$\omega_2 = \arcsin[(\rho_1 \sin \omega_1)/\rho_I]. \tag{9}$$

So far, we can obtain s_I's phase, i.e., φ_I, by using $\varphi_I = \phi_0 - \omega_2$, which in turn determines the phase coefficients $\theta_1, \theta_2, \cdots, \theta_M$ of the M reflective elements in IRS according to $\tilde{\varphi}_I^{(i)} = \varphi_I - \theta_i$ where $\tilde{\varphi}_I^{(i)}$ is a known variable (see the discussion below Eq. (8)).

Note that both ϕ_0 and φ_I are phases, so when calculating the angle of the triangle, it is important to take their positive or negative status into account. Depending on whether they are positive or negative, different situations may arise when solving for φ_I based on $\varphi_I = \phi_0 - \omega_2$. To better understand the above phenomenon, we define the phase difference between s_1 and x_0 as $\varphi_\delta = \varphi_1 - \phi_0$. The solution for φ_I is illustrated in Fig. 4 for four different cases, i.e., $\varphi_\delta \in (-\pi, -\pi/2]$, $\varphi_\delta \in (-\pi/2, 0]$, $\varphi_\delta \in (0, \pi/2]$, and $\varphi_\delta \in (\pi/2, \pi]$. As Fig. 4(a) shows, when $\varphi_\delta \in (-\pi, -\pi/2]$, the equation $\varphi_I = \pi - (-\phi_0) - \omega_2$ can be derived from the triangle $\triangle OXP$ with consideration of the positive or negative status of both ϕ_0 and φ_I (which are both in the interval $(-\pi, \pi]$). In other words, we have $\varphi_I = \phi_0 - \omega_2 + \pi$. Likewise, in Figs. 4(b), 4(c), and 4(d), we can derive the expression for φ_I by analyzing the relationship between the interior and exterior angles of the triangle $\triangle OXP$.

We present in Table II the relationships between ω_2, ϕ_0, and φ_I under various intervals of φ_δ.

Upon obtaining s_I's phase φ_I, we can compute θ_i ($i \in \{1, 2, \cdots, M\}$) according to Eq. (10):

$$\theta_i = \varphi_I - \tilde{\varphi}_I^{(i)}, \tag{10}$$

TABLE II

THE RELATIONSHIPS BETWEEN ω_2, ϕ_0, AND φ_I UNDER VARIOUS INTERVALS OF φ_δ

φ_δ	$(-\pi, -\pi/2]$	$(-\pi/2, 0]$	$(0, \pi/2]$	$(\pi/2, \pi]$
φ_I	$\phi_0 - \omega_2 + \pi$	$\phi_0 + \omega_2$	$\phi_0 - \omega_2$	$\phi_0 + \omega_2 - \pi$

where $\tilde{s}_I^{(i)}$'s phase, $\tilde{\varphi}_I^{(i)}$, is known (see the discussion below Eq. (8)). The M reflected interferences should align with each other at the PUE, so that $\varphi_I^{(1)} = \cdots = \varphi_I^{(M)} = \varphi_I$ can hold. With the calculated θ_i ($i \in \{1, 2, \cdots, M\}$), IRS-IE can generate an equivalent reflected interference to interact with the direct interference at the PUE, which can then recover its desired data from the mixed interference.

When there are multiple MUEs and one PUE, the MBS needs to generate multiple orthogonal beams towards its subscribers. Consequently, the PUE is subjected to multiple disturbances. However, by exploiting interactions among wireless signals, we can aggregate these multiple interferences into one effective disturbance [36] at the PUE and directly apply our method. When there are multiple PUEs and one MUE, we can't generate multiple reflected interferences interacting with the disturbance from the MBS towards each PUE and produce mutually orthogonal transmissions at multiple PUEs. In such a case, we need to employ multi-user scheduling method [37] to allow one PUE to receive its signal at a time. This way, the multi-PUE situation is simplified to a single-PUE case, enabling the application of our method.

IRS-IE offers advantages over other existing schemes in several aspects. First, IRS-IE does not require transmit power for interference exploitation. In contrast, both IN and IRC require additional power consumption for transmitting neutralizing and recycling signals, respectively. Second, both IN and IRS-assisted interference cancellation (IRS-IC) focus on mitigating interference power rather than exploiting it (an in-depth comparison of IRS-IE and IRS-IC is provided in Appendix A). In contrast, IRS-SE effectively utilizes both direct and reflected interferences to enhance the desired transmission. Third, unlike cooperative transmission mechanisms such as coordinated multi-point (CoMP), IRS-IE eliminates the need for bi-directional transmit data sharing (i.e., from PBS to MBS, and vice versa) and complex Tx-side cooperative signal processing. Additionally, IRS-IE does not alter the transmission performance of the macro communication pair, distinguishing it from cooperative transmission.

It is worth noting that IRS-IE requires symbol-level control of IRS's reflection coefficients, posing a challenge to its practical implementation. To the best of our knowledge, the response time of the IRS to the phase control signaling is determined by the physical and electrical characteristics of the IRS, which are beyond the scope of this work. Nevertheless, in practical use, we can reduce the symbol rate of the pico-transmission to an integral fraction (e.g., $1/\xi$ where ξ is a positive integer) of the interference symbol rate to align with the adjusting speed of the IRS. In this case, only one out of ξ interference symbols is utilized for the pico-transmission.

V. EXTENDED DESIGN OF IRS-IE

We presented above the IRS-IE design, demonstrating that the PUE can recover the desired data from the mixed inter-

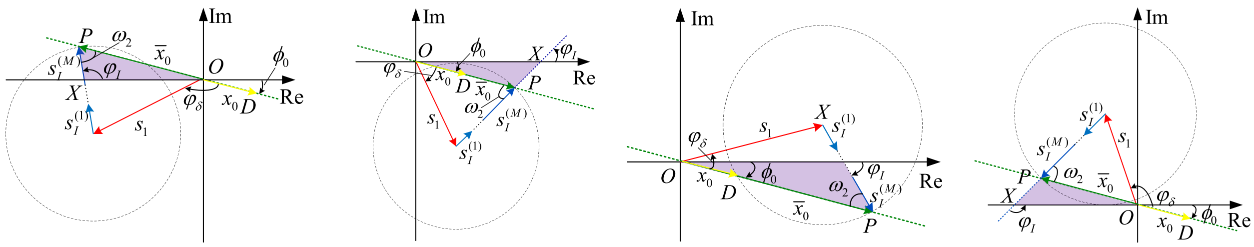

(a) $\varphi_\delta \in (-\pi, -\pi/2]$. (b) $\varphi_\delta \in (-\pi/2, 0]$. (c) $\varphi_\delta \in (0, \pi/2]$. (d) $\varphi_\delta \in (\pi/2, \pi]$.

Fig. 4. Illustration of calculation of ψ_i under various φ_δs.

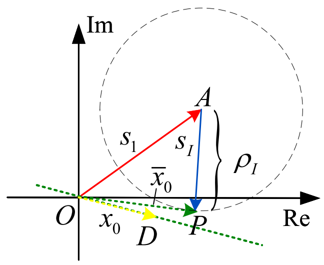

Fig. 5. Illustration of the infeasibility of IRS-IE.

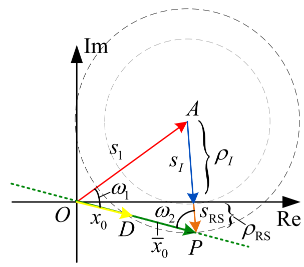

Fig. 6. Illustration of PBS-assisted IRS-IE.

ference under the assumption of MPSK. However, in practice, the direct and reflected interferences may experience random channel fading, making it challenging for the PUE to recover the desired data information. Additionally, the macro and pico communication pairs may employ different modulation schemes. In this section, we will first present a measurement to enhance the feasibility of IRS-IE, and then explore its application to scenarios where the communicating pairs utilize M-ary quadrature amplitude modulation (MQAM).

A. PBS-Assisted IRS-IE

Before delving into details, we first illustrate in Fig. 5 a scenario where the PUE is unable to accurately recover its desired data from the mixed interference.

As the figure shows, the spatial characteristics of the direct interference s_1 and the desired data x_0 are very different, and the strength of the reflected interference s_I is weak. As a result, the circle centered at A and with radius ρ_I does not intersect the line determined by x_0, indicating that the PUE cannot recover x_0 accurately from the mixed interference $\bar{x}_0$. However, since both x_0 and s_1 are known, we can enhance s_I to enable PUE to extract its desired data from the mixed signal. In what follows, we will present the measurement to enhance the feasibility of IRS-IE, namely, *PBS-assisted IRS-IE*.

In the previous design of IRS-IE, the PBS did not transmit any signal. However, in practice, the PBS can generate and send a recycling signal [11], denoted as s_{RS}, to the PUE. s_{RS} carries the interference data x_1 (the explanation of allowing PBS to transmit x_1 instead of x_0 is provided in Appendix B), which is pre-processed by the PBS. The pre-processing coefficient and the reflection coefficients of IRS elements need to be jointly designed based on $\boldsymbol{H}_{10}$, $\boldsymbol{H}_0$, $\boldsymbol{H}_{I0}$, $\boldsymbol{H}_{1I}$, x_1, and x_0.

According to the above design principle, we can rewrite Eq. (3) as:

$$\boldsymbol{y}_0 = \sqrt{\alpha P_{t_1}}\boldsymbol{H}_{10}\boldsymbol{p}_1 x_1 + \sqrt{\eta P_{t_1}}\sum_{i=1}^{M}\boldsymbol{h}_{I0}^{(i)}\psi_i e^{j\theta_i}\boldsymbol{h}_{1I}^{(i)}\boldsymbol{p}_1 x_1 + \sqrt{P_{t_0}}\boldsymbol{H}_0\boldsymbol{p}_{RS}x_1 + \boldsymbol{z}_0, \tag{11}$$

where the third term on the RHS denotes the recycling signal sent from the PBS. The unit vector $\boldsymbol{p}_{RS} = \boldsymbol{p}_0 e^{j\theta_{RS}}$ is the precoder at the PBS, where $\boldsymbol{p}_0$ can be obtained in terms of $\boldsymbol{H}_0$ (e.g., singular value decomposition (SVD) based precoding, please refer to the first paragraph in Section VI) and θ_{RS} represents a phase offset applied to $\boldsymbol{p}_0$. Then, Eq. (5) becomes:

$$\sqrt{\alpha P_{t_1}}\boldsymbol{f}_0^H\boldsymbol{H}_{10}\boldsymbol{p}_1 x_1 + \sqrt{\eta P_{t_1}}\sum_{i=1}^{M}\boldsymbol{f}_0^H\boldsymbol{h}_{I0}^{(i)}\psi_i e^{j\theta_i}\boldsymbol{h}_{1I}^{(i)}\boldsymbol{p}_1 x_1 + \sqrt{P_{t_0}}\boldsymbol{f}_0^H\boldsymbol{H}_0\boldsymbol{p}_{RS}x_1 = \lambda x_0. \tag{12}$$

We use Fig. 6 to illustrate the principle of PBS-assisted IRS-IE. As the figure shows, the interactions of s_1, s_I, and s_{RS} yield $\bar{x}_0 = \lambda x_0$, indicating that the PUE can retrieve its intended data from the mixed signals consisting of the direct interference, reflected interference, and the recycling signal.

We set $s_{RS} = \sqrt{P_{t_0}}\boldsymbol{f}_0^H\boldsymbol{H}_0\boldsymbol{p}_{RS}x_1 = \rho_{RS}e^{j\varphi_{RS}}$, where the amplitude ρ_{RS} is a real number that can be calculated based on P_{t_0}, h_0, and x_1, while the phase $\varphi_{RS} \in (-\pi, \pi]$ is affected by θ_{RS}. Therefore, we need to jointly design θ_i ($i \in \{1, 2, \cdots, M\}$) and θ_{RS} to make s_{RS} and the reflected interference be in-phase at the PUE. This alignment facilitates an expanded radius for the circle centered at A, enabling it to intersect the line defined by x_0. Then, we can have:

$$\sin\omega_2 = \rho_1/(\rho_I + \rho_{RS})\sin\omega_1. \tag{13}$$

The solution for θ_i and θ_{RS} is the same as that for θ_i presented in Section IV, and hence its details are omitted.

Note that the power of PBS can be utilized for both recycling signal and desired signal transmission. Therefore, by optimally allocating the power of PBS, we can enhance the transmission performance of the PUE while ensuring

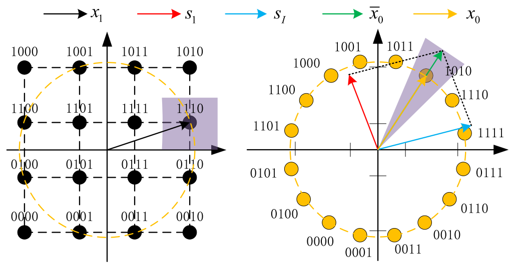

(a) 16QAM (b) 16PSK

Fig. 7. DAI-assisted IRS-IE under 16QAM interference.

the feasibility of IRS-IE. However, due to space limitation, we omit the discussion of the optimal power allocation of the PBS which will be part of our future work.

B. Application of IRS-IE Under MQAM

So far, we assumed that the MBS employs MPSK modulation, and the PUE treats the mixed interference as an MPSK signal for demodulation. Thus, IRS-IE only needs to consider the phase of x_0. When MQAM modulation is adopted at MBS, both amplitude and phase represent data information. In this situation, when the PUE treats its perceived mixed interference as an MQAM modulated signal, the reflected interference must interact with the direct one to produce a mixed interference with accurate amplitude and phase characteristics. Consequently, the IRS-IE may need to amplify the incident signal at the IRS, requiring the amplitude coefficient to be larger than 1. In such a case, an active IRS is necessary. Then, the value of λ in Eqs. (5)–(7) should be 1. So, we can rewrite Eq. (7) as:

$$s_1 + \sum_{i=1}^{M} s_I^{(i)} = x_0. \tag{14}$$

From Eq. (14), we can determine the target amplitude and phase of the reflected interference $s_I = \sum_{i=1}^{M} s_I^{(i)}$. Then, the reflection coefficient of each IRS element, denoted as $\psi_i e^{j\theta_i}$ where ψ_i and θ_i are the amplitude and phase coefficients, respectively, can be calculated according to Eqs. (8) and (10).

If a passive IRS is still employed in the IRS-IE, as IRS-IE can only control the reflected interference, and the intensity of the reflected interference is limited by the PRP of MBS, IRS elements, and PUE, generating the required reflected interference with desired amplitude and phase becomes challenging. To address the above issue, we propose a method called *discarding amplitude information* (DAI) to enable PUE to process an interfering MQAM modulated signal as an MPSK signal for demodulation and retrieve the desired data therein.

Fig. 7 takes the 16QAM and 16PSK as an example to show the principle of DAI. As the figure shows, the constellation points correspond to waveforms with various phases and amplitudes. For ease of implementation and fair comparison, we equalize the average power of constellation points for both 16QAM and 16PSK. Consequently, there are 8 constellation points in 16QAM that have the same amplitude as the constellation points in 16PSK, as illustrated in Fig. 7(a).

Under DAI, when the MBS adopts 16QAM, the PUE demodulates its perceived mixed interference using 16PSK. Without loss of generality, we let the desired data x_1 for MUE and x_0 for PUE be "1110" and "1010", respectively. Then, the interference from the MBS to PUE can be represented by a red arrow, s_1, as shown in Fig. 7(b). At the MUE, the desired signal transmitted from the MBS is decoded to obtain x_1, as depicted by the black arrow in Fig. 7(a). With proper design of the reflection coefficients of IRS elements, a reflected interference s_I (the blue arrow in Fig. 7(b)) can be produced. s_I interacts with s_1, causing the phase of $\bar{x}_0$ (the green arrow in Fig. 7(b)) obtained by PUE from post-processing the mixed interference to fall within the range of the constellation point "1010" (i.e., x_0, the orange arrow in subfigure 7(b)) in 16PSK. This way, the requirement for the specific amplitude of the mixed interference under MQAM is eliminated, making the construction of reflected interference easier. In summary, with the assistance of DAI, IRS-IE only needs to construct a reflected interference that can steer the direct interference to the correct phase, without the need to consider the amplitude of the target constellation. Then, the PUE can recover its desired data according to the method presented in Section IV.

It is worth noting that in the current design of IRS-IE, as described in Sections IV and V-B, the modulation order of the interference and the demodulation order at the interfered Rx are identical. However, in practical use, the modulation and demodulation orders can be different. By leveraging inter-BS cooperation, the MBS can control the IRS to generate a reflected interference component to interact with the direct one at the PUE, yielding a desired signal waveform that the PUE intends to process afterward. The order of the combined signal matches the demodulation order at the PUE.

VI. Evaluation

We now use MATLAB simulation to evaluate the performance of the proposed IRS-IE. First, we will simulate the feasibility of the proposed IRS-IE. We will then compare IRS-IE with other typical IM methods in terms of the spectral efficiency (SE) of the desired transmission. Without loss of generality, we adopt a spatially uncorrelated Rayleigh flat fading channel model to model the elements of the above matrices as independent and identically distributed zero-mean unit-variance complex Gaussian random variables. We assume that all UEs experience block fading, i.e., channel parameters remain constant in a block consisting of several time slots and vary randomly between successive blocks. We set $N_{T_1} = N_{T_0} = N_{R_1} = N_{R_0} = 2$. Both the macro and pico communications employ BPSK modulation/demodulation. Taking singular value decomposition (SVD) based precoding and filtering as an example, we apply SVD to $\boldsymbol{H}_0$ and $\boldsymbol{H}_1$ to obtain $\boldsymbol{H}_0 = \boldsymbol{U}_0\boldsymbol{\Lambda}_0\boldsymbol{V}_0^H$ and $\boldsymbol{H}_1 = \boldsymbol{U}_1\boldsymbol{\Lambda}_1\boldsymbol{V}_1^H$, respectively. Then, we employ $\boldsymbol{p}_0 = \boldsymbol{v}_0^{(1)}$ and $\boldsymbol{p}_1 = \boldsymbol{v}_1^{(1)}$ as the precoding vectors at PBS and MBS, while $\boldsymbol{f}_0 = \boldsymbol{u}_0^{(1)}$ and $\boldsymbol{f}_1 = \boldsymbol{u}_1^{(1)}$ are the filter vectors at PUE and MUE, where $\boldsymbol{v}_0^{(1)}$, $\boldsymbol{v}_1^{(1)}$, $\boldsymbol{u}_0^{(1)}$, and $\boldsymbol{u}_1^{(1)}$ represent the first column vectors of $\boldsymbol{V}_0$, $\boldsymbol{V}_1$, $\boldsymbol{U}_0$, and $\boldsymbol{U}_1$, respectively.

Next, we will first simulate the impact of M, power utility factor α, and η on the feasible probability of IRS-IE. Let

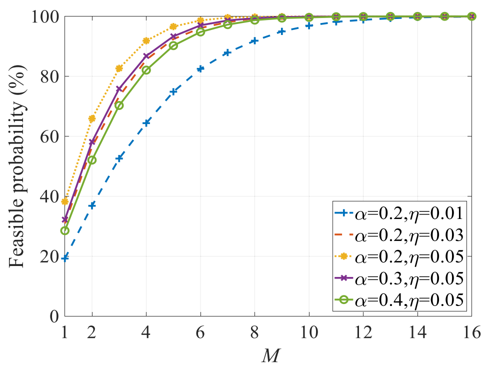

Fig. 8. Variation of the feasible probability of IRS-IE with M under various αs and ηs.

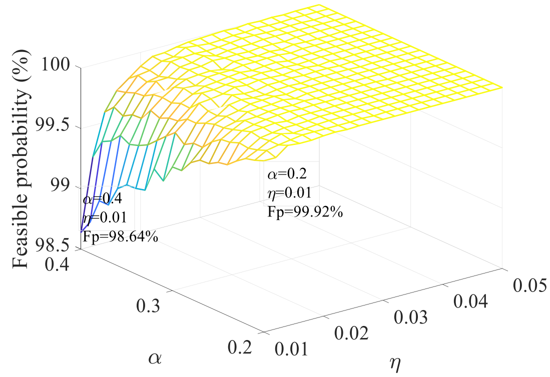

Fig. 9. The feasible probability of IRS-IE under $M = 16$ and various αs and ηs.

P_{T_1} and P_{T_0} be the transmit power of MBS and PBS, respectively. According to the modified signal transmission model in Section III-B, the effective power of MBS radiating to MUE is denoted as P_{t_1}, and the effective power of MBS radiating to PUE is $\tilde{P}_{t_1} = \alpha P_{t_1}$, where $\alpha \in [0.2, 0.4]$. Additionally, the effective power of PBS radiating to PUE is denoted as P_{t_0}. Since the relationships between P_{T_0} and P_{T_1}, as well as P_{t_0} and P_{T_0}, only affect the simulations of Figs. 10-12, we will provide their details prior to the presentation of these figures. The effective power of the reflected interference that PUE receives from each IRS element is ηP_{t_1}, where $\eta \in [0.01, 0.05]$. α and η are determined by such factors as the position and PRP of MBS, PBS, and IRS. Using Monte Carlo simulation, we set the number of simulation runs to 2×10^5. In each simulation, we randomly generate $\boldsymbol{h}_0$ and $\boldsymbol{h}_1$, and evaluate the performance of IRS-IE under the above parameter settings.

Fig. 8 plots the impact of the number of IRS elements M on the feasible probability (Fp) of IRS-IE (i.e., the probability that $\bar{x}_0$ is aligned with x_0) under various αs and ηs. As the figure shows, given fixed α and η, the Fp of IRS-IE increases as M grows, eventually reaching 1. This is because when M is small, the interference power gathered by IRS is also small, making high the probability that the PUE cannot recover its desired data from the mixed interference. As M grows larger, the strength of reflected interference increases, hence improving the feasibility of IRS-IE. Given fixed α and M, the Fp of IRS-IE grows as η increases. This is because a larger η leads to the collection of more interference power by the IRS, increasing the intensity of reflected interference (i.e., ρ_I) and thus increasing the probability that the PUE can retrieve its desired data from the mixed interference. When η and M are fixed, the Fp of IRS-IE decreases with an increase of α. This is because a larger α leads to a stronger direct interference s_1, and achieving IRS-IE requires a stronger reflected interference s_I (as shown in Fig. 5, a circle centered at A with a larger radius is required). As a result, the Fp of IRS-IE decreases. Moreover, we can observe from Fig. 8 that the Fp IRS-IE saturates as M approaches 16. This indicates that under $\alpha \in \{0.2, 0.3, 0.4\}$ and $\eta \in \{0.01, 0.03, 0.05\}$, increasing M beyond 16 does not enhance the IRS's ability further to gather more interference power. Therefore, in the following evaluation, we set $M_{\max} = 16$.

TABLE III

THE IMPACT OF INCREASING M, α, AND η ON THE FP OF IRS-IE

Parameter	M	α	η
Variation of Fp	$\nearrow$	$\searrow$	$\nearrow$

Fig. 9 plots the impact of α and η on the feasible probability of IRS-IE under $M = M_{\max} = 16$. Since under $\alpha \in [0.2, 0.4]$ and $\eta \in [0.01, 0.05]$, an IRS with 16 elements can gather sufficient interference power and forward it to the PUE, the Fp of IRS-IE under these parameter settings exceeds 98.64%. At $\alpha = 0.2$ and $\eta = 0.01$, the Fp reaches approximately 99.92%. At $\alpha = 0.4$ and $\eta = 0.05$, it achieves around 100%. Moreover, for $\alpha = 0.2$ and $\eta = 0.05$, the Fp is 100%. As the figure shows, the feasibility of IRS-IE improves as α decreases and η increases. This is because a lower α reduces the required strength of the reflected interference, while a higher η enables the IRS to collect more interference power. As a result, the Fp of IRS-IE increases until 100%.

We present in Table III the impact of increasing M, α, and η on the feasible probability of IRS-IE, where the notations $\nearrow$ and $\searrow$ represent an increase and decrease in Fp, respectively.

In what follows, we simulate and compare the spectral efficiency (SE) of IRS-IE with other existing IM methods, including zero-forcing (ZF) reception, interference neutralization (IN) [7], IRS-assisted interference cancellation (IRS-IC), and interference recycling (IRC) [11]. Here, IRS-IC adjusts the reflection coefficient of the IRS to ensure that the reflected interference has the opposite phase to the direct interference at the desired/interfered PUE. For the pico-communication pair, PBS uses $\boldsymbol{p}_0 = \boldsymbol{v}_0^{(1)}$ for precoding and PUE employs $\boldsymbol{f}_0 = \boldsymbol{u}_0^{(1)}$ as the filter vector. This approach helps suppress the influence of interference on the desired transmission. However, since IRS cannot amplify its incident signal, we cannot guarantee the strength of the reflected interference to be identical to its direct counterpart. As a result, there may be residual interference that could potentially degrade the reception at the desired Rx. Moreover, transmission without IM, namely non-IM, is also simulated for comparison, where the pico-communication pair perform data transmission the same as that in IRS-IC. Note that when IRS-IE, IN, and IRC become infeasible, we switch to non-IM to compute PUE's SE. Although P_{T_1} (ranges from 43dBm to 49dBm) is several or even hundreds of times that of P_{T_0} (ranges

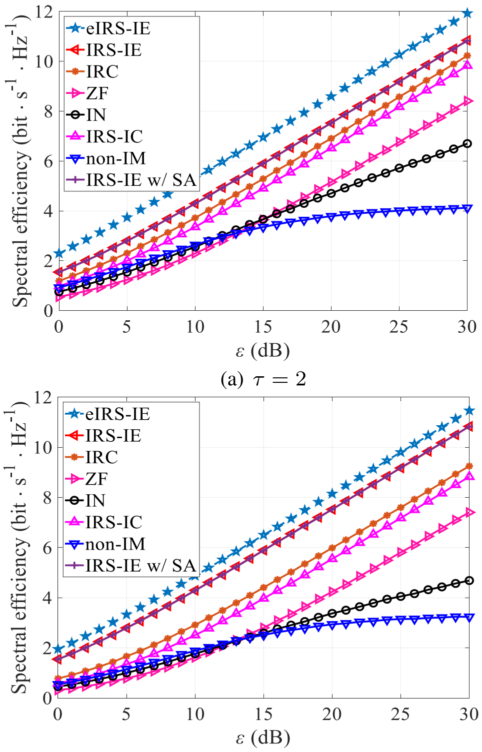

(a) $\tau = 2$

(b) $\tau = 4$

Fig. 10. Comparison of PUE's SE under various εs and $\tau \in \{2, 4\}$.

from 24dBm to 37dBm) [28], due to the inverse proportion of the path loss to the square of distance (MBS is far from PUE, about a few thousand meters, while PBS is close to PUE, about a few hundred meters) [38], we comprehensively consider path loss within the transmit power P_{T_1} and P_{T_0} of MBS and PBS, and set $P_{T_1} = \tau P_{T_0}$ (P_{T_1} and P_{T_0} in the following text also include path loss), where $\tau \in [1, 4]$ in the simulation. We define the normalized value of MBS's transmit power to noise as $\varepsilon = 10\lg(P_{T_1}/\sigma_n^2)$dB, where σ_n^2 represents additive white Gaussian noise (AWGN) power, and set $\varepsilon \in [0, 30]$dB. Considering the fact that most of MBS's power is sent to the MUE (i.e., P_{t_1}), while a relatively small amount of MBS's power is received by the PUE (consisting of a direct component, αP_{t_1}, and a reflected component, $M\eta P_{t_1}$, via the IRS), without loss of generality, we set $P_{t_1} = 0.6P_{T_1}$, $\alpha = 0.33$ and $\eta = 0.015$ (note that $0.33P_{t_1} = 0.2P_{T_1}$ and $0.015P_{t_1} = 0.009P_{T_1}$), and take $M = M_{\max} = 16$.

Fig. 10 shows the variation of PUE's SE obtained by different methods with ε when τ takes different values. It should be noted that when using IRS-IE, we assume PBS does not send any signals, i.e., the power overhead of PBS is 0, while when using other methods, the transmit power of PBS is P_{T_0}. For fairness, we also simulate an enhanced version of IRS-IE, namely eIRS-IE, with which PBS sends a recycling signal with transmit power P_{T_0} (as discussed in Section V-A), which is denoted as eIRS-IE. Additionally, we plot PUE's SE of IRS-IE with single antenna configuration, namely IRS-IE w/ SA.

Fig. 10(a) compares the PUE's SE of different methods under various εs and $\tau = 2$. As the figure shows, eIRS-IE achieves the highest SE, followed by IRS-IE and IRS-IE w/ SA, and then by IRC, next by IRS-IC. When ε is small, the SE performance of ZF and IN is inferior to that of non-IM. This is because the noise power is greater than the interference/desired signal at this time, i.e., noise is the key factor affecting SE, and ZF and IN can cause a loss in the desired signal transmission performance when managing interference (ZF reduces the desired signal received by the PUE from the PBS while eliminating interference; IN needs to consume the transmit power of PBS to offset interference at the PUE). Therefore, the SE benefits brought by eliminating interference are less than the SE loss caused by interference management, resulting in a lower SE than that of non-IM. As ε increases, the SE of ZF and IN improves and eventually outperforms that of non-IM. This is because the noise power is smaller than the interference/desired signal, and thus interference becomes a key factor affecting SE. As a result, the increase in PUE's SE achieved by using IM exceeds the SE loss incurred by IM costs, yielding higher SE of ZF and IN than that of non-IM.

Since eIRS-IE utilizes both direct and reflected interference and also allows PBS to send a recycling signal to PUE, the mixed signal at PUE is equivalent to the desired signal of greater strength, thus maximizing the SE of PUE obtained by eIRS-IE. The SE of IRS-IE w/ SA overlaps with that of IRS-IE using multiple antennas. This is due to the fact that under IRS-IE, PBS does not transmit any signal, and the transmission from MBS is directed towards MUE rather than PUE. Therefore, while employing multiple antennas can provide beamforming gain, it does not contribute to the enhancement of PUE's SE under IRS-IE. IRS-IE is superior to IRC in PUE's SE. This is because the reflection coefficient matrix of IRS can modify the channel so that all the reflected interference components are in-phase at the PUE, resulting in a reflected interference which is stronger than the recycling signal, and thus IRS-IE outperforms IRC. As for the comparison between IRC and IRS-IC, IRC converts interference using a recycling signal, thus utilizing the interference for desired transmission. In contrast, IRS-IC leverages the reflected disturbance for interference suppression. Therefore, IRC can yield a higher PUE's SE than IRS-IC. As mentioned before, both ZF and IN cause a loss of desired signal's transmission performance when managing interference, while both IRS-IE and IRC leverage the power and data carried by interference, so they achieve a higher SE of PUE than ZF and IN.

Fig. 10(b) gives the variation of the PUE's SE obtained using different methods under various εs when $\tau = 4$. As the figure shows, the variation pattern of the SE curves with different methods is similar to that in Fig. 10(a). However, since the transmit power of PBS under $\tau = 4$ is weaker than that under $\tau = 2$, the SE curves of the studied methods degrade more or less in subfigure (b) compared to subfigure (a). IRS-IE's SE is the least affected, followed by eIRS-IE's SE. Fig. 11 shows a further analysis of the impact of τ on the SE performance of various IM methods.

Fig. 11 plots the variation of PUE's SE with τ under different methods and various εs. In both subplots, the SE of PUE yielded by IRS-IE shows a very slight decrease as ε grows. This is because given fixed ε, P_{T_1} is a deterministic value while P_{T_0} reduces as τ increases. Moreover, although the Fp of IRS-IE is high (when IRS-IE is feasible, the SE

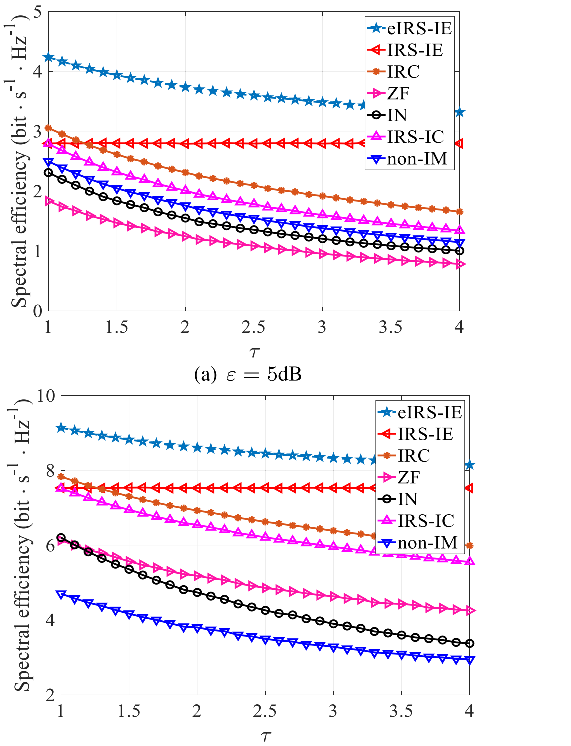

(a) $\varepsilon = 5$dB

(b) $\varepsilon = 20$dB

Fig. 11. Comparison of PUE's SE under various τs and $\varepsilon \in \{5\text{dB}, 20\text{dB}\}$.

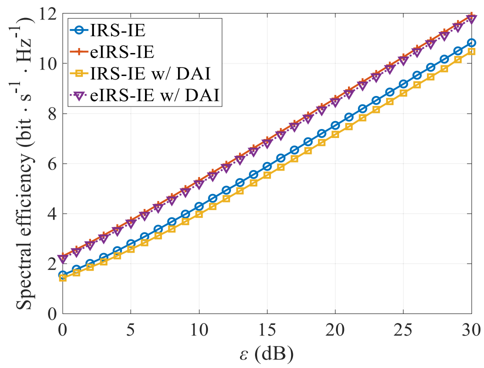

Fig. 12. Comparison of PUE's SE under various εs.

of PUE is only affected by P_{T_1}), there is still a very low probability of infeasibility (in which PBS employs non-IM to transmit to PUE, and the SE of non-IM decreases as τ increases). Combining the above analyses, the SE of IRS-IE decreases slightly as τ grows. In contrast, since the PUE's SE of the other methods depends on P_{T_0}, it shows a obvious reduction as τ increases.

Fig. 11(a) compares the PUE's SE of different methods under various τs and $\varepsilon = 5$dB. As shown in the figure, excluding IRS-IE which has been discussed in the previous paragraph, eIRS-IE yields the highest SE, followed by IRC, IRS-IC ranks third, non-IM ranks fourth, and IN ranks fifth, while ZF's SE is the smallest. When τ is very low, the interference power for utilization is small, making IRS-IE's SE inferior to IRC's. As τ increases, IRS-IE's SE exceeds IRC's. The analysis can be found in the discussion about Fig. 11. Fig. 11(b) compares the PUE's SE under various τs and $\varepsilon = 20$dB. As the figure shows, eIRS-IE achieves the highest SE, followed by IRC, IRS-IC ranks third, ZF ranks fourth, and IN ranks fifth, while non-IM has the lowest SE. A detailed analysis of these results can be found in the discussion of Fig. 10, and is thus omitted here.

Fig. 12 compares the PUE's SE of IRS-IE, eIRS-IE, IRS-IE w/ DAI, and eIRS-IE w/ DAI. We assume that the PBS intends to transmit to PUE employing 16PSK modulation. As for the MBS, it employs 16PSK for transmission under IRS-IE and eIRS-IE. This is because both methods require the interfered transmission pair to use the same modulation scheme as the interfering source. However, when using IRS-IE w/ DAI and eIRS-IE w/ DAI, the MBS uses 16QAM for transmission. This is because, with the assistance of DAI, the interfered transmission pair is able to use a modulation scheme that differs from the interfering source. The remaining parameter settings are the same as those given in Fig. 10(a). Although we take 16QAM/16PSK as an example to compare different methods, similar results can be obtained with other modulation schemes as well. Due to space limitation, we omit the specific results in this discussion. As the figure shows, the SE of IRS-IE w/ DAI and eIRS-IE w/ DAI is slightly lower than that of IRS-IE and eIRS-IE, respectively. This is because, in the methods with the assistance of DAI, PUE discards the amplitude information of the interference. Consequently, this leads to a loss in the quality of the desired signal and results in a degraded SE performance. Note that in the eIRS-IE w/ DAI, the PBS also sends a recycling signal to the PUE. This allows for compensation of the performance loss caused by discarding the amplitude information of the interference under DAI. Therefore, the difference in SE between eIRS-IE w/ DAI and eIRS-IE is negligible.

Lastly, we compare the system SE of the proposed schemes with other mechanisms, including IRS-IC, IRC, IN, ZFBF, cooperative transmission (CT), and non-IM. Since ZFBF requires that the total number of receive antennas should not exceed the number of transmit antennas, we set $N_{T_0} = N_{T_1} = 2$ and $N_{R_0} = N_{R_1} = 1$ when our methods are compared with ZFBF. As for CT, we assume that the transmission from PBS to MUE is negligible. In this scenario, only MBS and PBS cooperatively transmit to PUE, PBS does not assist in the macro transmission; that is, PBS only transmits x_0.

First, we present in Table IV the effective transmit power, which is the original transmit power adjusted by the transmit/receive PRP, at the communication entities along the link, for MUE and PUE via various transmission links. The second column of Table IV illustrates the scenario where PBS transmits signal, whereas the third column depicts the case where PBS does not transmit any signal. For example, μP_{t_1} represents the power transmitted from MBS to MUE via IRS, while νP_{t_0} indicates the power transmitted from the PBS to MUE. Since the main lobe of PUE's PRP is aligned with the PRP of its intended transmitter, i.e., PBS, when PBS is transmitting a signal, it is no longer aligned with the main lobe of the IRS, as it was in the case where PBS was not transmitting any signal. Therefore, we use $\hat{\alpha} P_{t_1}$ and $\hat{\eta} P_{t_1}$ to denote the effective power received by PUE from PBS and from MBS via IRS when PBS is transmitting a signal,

TABLE IV
EFFECTIVE POWER FOR MUE/PUE WITH AND WITHOUT PBS TRANSMITTING A SIGNAL

Transmission link	Effective power w/ PBS's transmission	Effective power w/o PBS's transmission
MBS-MUE	$P_{t_1} = 0.6P_{T_1}$	$P_{t_1} = 0.6P_{T_1}$
PBS-PUE	$P_{t_0} = 0.6P_{T_0}$	—
MBS-PUE	$\hat{\alpha}P_{t_1} = 0.1P_{T_1}$	$\alpha P_{t_1} = 0.2P_{T_1}$
MBS-IRS-PUE	$\hat{\eta}P_{t_1} = 0.0045P_{T_1}$	$\eta P_{t_1} = 0.009P_{T_1}$
MBS-IRS-MUE	$\mu P_{t_1} = 0.0018P_{T_1}$	$\mu P_{t_1} = 0.0018P_{T_1}$
PBS-MUE	$\nu P_{t_0} = 0.06P_{T_0}$	—

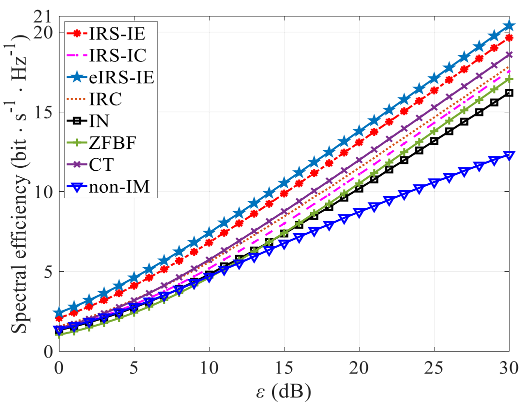

Fig. 13. Comparison of system's SE under various εs for $\tau = 4$.

in contrast to αP_{t_1} and ηP_{t_1} in the second column. Note that the powers in the second and third columns of the table satisfy $P_{t_1} + \hat{\alpha}P_{t_1} + \sum_{i=1}^{M} \hat{\eta}P_{t_1} + \sum_{i=1}^{M} \mu P_{t_1} \leq P_{T_1}$ and $P_{t_0} + \nu P_{t_0} \leq P_{T_0}$ and $P_{t_1} + \alpha P_{t_1} + \sum_{i=1}^{M} \eta P_{t_1} + \sum_{i=1}^{M} \mu P_{t_1} \leq P_{T_1}$, respectively.

Fig. 13 plots the variation of average system SE of with ε. As the figure shows, eIRS-IE yields the highest SE, followed by IRS-IE, CT, IRC, IRS-IC, ZFBF, and IN, while non-IM outputs the lowest SE. The analysis is as follows. Under CT, MBS needs to design a precoding matrix for simultaneously transmitting two signals to both MUE and PUE, leading to a reduced alignment with $\boldsymbol{H}_1$ and a decrease in the beamforming gain for the MUE. In contrast, IRS-IE and eIRS-IE utilize interference to realize/enhance the pico transmission without sacrificing the macro transmission's performance. As a result, the system's SE under CT is lower than that under our methods. When comparing CT with IRC, the MBS can transmit a relatively strong desired signal to the PUE, which is superimposed with the desired signal transmitted by the PBS. In contrast, IRC's performance is affected by the power of PBS, i.e., P_{T_0}, which determines the outcome of the interaction between the recycling signal and the interference. Since P_{T_0} is much smaller than P_{T_1}, IRC's SE performance is inferior to that of CT. As for ZFBF, it mitigates interference among current transmissions through precoding at both MBS and PBS. However, this approach incurs beamforming gain reduction and SE loss for both MUE and PUE. Consequently, ZFBF yields lower SE compared to IRS-IE, eIRS-IE, CT, and IRC. Moreover, IRS-IC leverages reflected interference for IM at PUE, while maintaining alignment of macro and pico transmissions with $\boldsymbol{H}_1$ and $\boldsymbol{H}_0$, its system SE surpasses that of ZFBF. A detailed analysis of the comparison between the other methods can be found in the discussions about Figs. 10(a) and 10(b) of our manuscript. Due to space limitations, we omit it here.

VII. CONCLUSION

In this paper, we proposed an *IRS-Assisted Interference Exploitation* (IRS-IE). In this method, the interfering source controls an IRS to reflect a portion of its interference to the interfered Rx, and the reflected interference can interact with the direct one at the interfered Rx so that the Rx can recover its desired data from the mixed interference. This way, interference utilization is realized. Our theoretical analysis and simulation results have shown that the proposed IRS-IE can effectively utilize the interference to significantly enhance the interfered communication-pair's performance.

APPENDIX A
COMPARISON OF IRS-IE AND IRS-IC

Here we demonstrate the advantages of IRS-IE over IRS-IC, assuming that the strength of the reflected interference for interference cancellation is equivalent to that for interference exploitation. In the analysis, we will consider three different situations as follows.

- First, we assume that the strength of the reflected interference is the same as that of the direct interference, as shown in Fig. 14(a), where $|\overrightarrow{OA}| = |\overrightarrow{AP_C}|$ holds. Here, $\overrightarrow{AP_C}$ denotes the reflected interference for IRS-IC. It can be easily seen that when we move P_C along the green dashed line where x_0 is located, to position P_E, we can obtain the reflected interference, denoted as $\overrightarrow{AP_E}$, for IRS-IE. That is, both IRS-IC and IRS-IE are feasible, but IRS-IC only mitigates the interference component, while IRS-IE can output a desired signal, denoted as $\overrightarrow{OP_E}$. As for the communication pair employing IRS-IC, additional power is required for data transmission. Note, however, in practice, the reflected interference may be stronger than the direct interference. In such a case, IRS-IC only utilizes a portion of the reflected interference to neutralize the direct counterpart, without producing any desired signal at the PUE. As for IRS-IE, it can perform even better by utilizing a stronger interference.
- Fig. 14(b) illustrates the scenario where the reflected interference is adequate for IRS-IE, but insufficient to mitigate the direct interference. In such a case, IRS-IE can yield a non-zero desired signal $\overrightarrow{OP_E}$. In contrast, IRS-IC is unable to counteract the interference even with the entire transmit power, let alone facilitate desired data transmission.

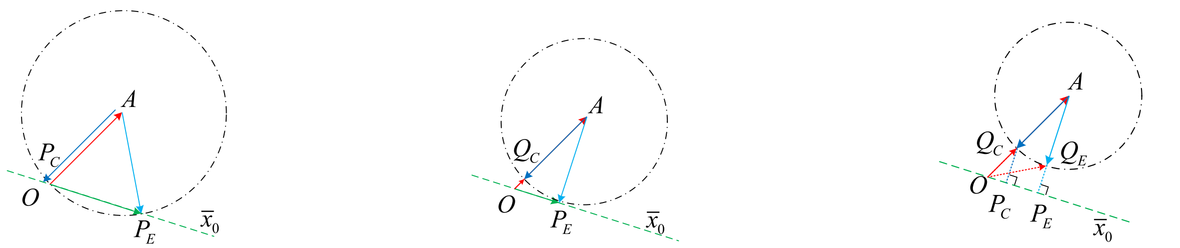

(a) Both IRS-IC and IRS-IE have solutions.

(b) Only IRS-IE has a solution.

(c) Neither IRS-IC nor IRS-IE has a solution.

Fig. 14. Comparison of IRS-IE and IRS-IC.

TABLE V
COMPARISON OF IRS-IE AND IRS-IC WITH FIXED TRANSMIT POWER AT MBS

Scenario	Residual intf. w/ IRS-IE	Residual intf. w/ IRS-IC	Desired sig. w/ IRS-IE	Desired sig. w/ IRS-IC
14(a)	0	0	$\overrightarrow{OP_E}$	0
14(b)	0	$\overrightarrow{OQ_C}$	$\overrightarrow{OP_E}$	0
14(c)	$\overrightarrow{OQ_E}$ ($\lvert\overrightarrow{P_EQ_E}\rvert < \lvert\overrightarrow{P_CQ_C}\rvert$)	$\overrightarrow{OQ_C}$	0	0

- Fig. 14(c) shows the situation where the reflected interference is insufficient for both IRS-IE and IRS-IC. In such a case, there exists a residual interference denoted as $\overrightarrow{OQ_C}$ under IRS-IC, and as for IRS-IE, the residual interference is denoted as $\overrightarrow{OQ_E}$. We project the residual interference onto $\bar{x}_0$. Since both points Q_C and Q_E lie on the circle centered at A with a radius $|\overrightarrow{AQ_E}|$ (or $|\overrightarrow{AQ_C}|$), it is evident that the influence of the residual interference, denoted as $\overrightarrow{P_EQ_E}$ with IRS-IE, on the desired signal, is less than that under IRS-IC, denoted as $\overrightarrow{P_CQ_C}$.

Based on the above analysis, we show the advantages of IRS-IE over IRS-IC. We use Table V to summarize the discussions above. Since deriving a closed-form expression to present the performance gap between IRS-IE and IRS-IC under various situations as shown in Fig. 14 is challenging and beyond the scope of this paper, we employ MATLAB simulation to statistically demonstrate the performance gap between the two schemes in Section VI.

APPENDIX B
DISCUSSION OF PBS TRANSMISSION BETWEEN x_1 AND x_0

In practice, the PBS can directly transmit x_0 to its serving Rx, instead of transmitting s_{RS} carrying x_1. Although the former strategy can avoid data sharing from MBS to PBS, it cannot yield as good reception performance as the latter. This will be illustrated in the following discussions.

We assume that the reflected interference is insufficient for effective interference exploitation, as depicted in Fig. 15. In this figure, we can see that the reflected interference $s_I = \overrightarrow{AB}$ is not strong (long) enough to intersect the green dashed line where x_0 is located. Then, under IRS-IE, the PBS generates $s_{RS} = \overrightarrow{BP_{x_1}}$ which aligns with s_I at the PUE, enabling the retrieval of the desired signal with a strength of $|\overrightarrow{OP_{x_1}}|$. If we allow the PBS to generate a signal carrying x_0 with the same strength of $\overrightarrow{BP_{x_1}}$ at the PUE, it becomes evident that a residual interference $\overrightarrow{OB}$ still exists, potentially impairing the desired transmission. In contrast, when using PBS to transmit x_1, there is no residual interference; in other words, interference has been successfully exploited. Based on the above analysis, when PBS transmits x_0 to assist IRS-IE, it still needs to eliminate the residual interference $\overrightarrow{OB}$. Then, the desired transmission in both cases is free from interference, allowing for a comparison between the scenarios where PBS transmits x_1 and x_0. To achieve this goal, as depicted in Fig. 15, a neutralizing signal, denoted as $\overrightarrow{CD}$ where C is the projection of B onto the green dashed line, with the opposite phase and same strength of $\overrightarrow{OB}$, can be employed. Therefore, PBS needs to allocate its transmit power for the generation of both $\overrightarrow{OP_{x_0}}$ and $\overrightarrow{CD}$ at the PUE. Note that generating the neutralizing signal still requires the MBS to share the information of x_1.

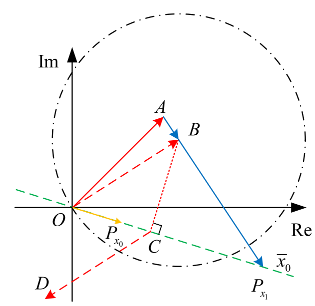

Fig. 15. Comparison of PBS transmission between x_1 and x_0.

When $|\overrightarrow{BP_{x_1}}| \le |\overrightarrow{OB}|$, PBS doesn't have enough power for both direct interference counteracting and x_0's transmission. When $|\overrightarrow{BP_{x_1}}| > |\overrightarrow{OB}|$, we apply the law of Cosines to triangle ΔOBP_{x_1} and can have:

$$|\overrightarrow{OB}|^2 + |\overrightarrow{OP}_{x_1}|^2 - 2|\overrightarrow{OB}||\overrightarrow{OP}_{x_1}|\cos\angle BOP_{x_1} = |\overrightarrow{BP}_{x_1}|^2 \tag{15}$$

where $\angle BOP_{x_1}$ represents the angle between $\overrightarrow{OB}$ and $\overrightarrow{OP}_{x_1}$. Since $\angle BOP_{x_1} \in (0, \frac{\pi}{2})$ holds,[3] we can get $|\overrightarrow{OB}|^2 +$

[3] When $\angle BOP_{x_1} \in (\frac{\pi}{2}, \pi)$, we can generate a reflected interference to recover $-x_0$ similar to the process used to recover x_0 under $\angle BOP_{x_1} \in (0, \frac{\pi}{2})$. Then, we can feed a polarity coefficient of -1 to the PUE for the correct retrieval of x_0.

$|\overrightarrow{OP}_{x_1}|^2 > |\overrightarrow{BP}_{x_1}|^2$ and obtain:

$$|\overrightarrow{OP}_{x_1}|^2 > |\overrightarrow{BP}_{x_1}|^2 - |\overrightarrow{CD}|^2 = |\overrightarrow{OP}_{x_0}|^2. \qquad (16)$$

That is, with the same transmit power, PBS transmitting x_0 to assist IRS-IE can only achieve inferior reception performance to that PBS transmitting x_1 to assist IRS-IE. Moreover, as aforementioned, since allowing the PBS to transmit x_0 cannot mitigate or utilize interference, interference data sharing from the MBS is still required for interference elimination.

References

[1] R. Anwar, K. Nishat, M. Ali, Z. Akhtar, H. Niaz, and I. A. Qazi, "Loss differentiation: Moving onto high-speed wireless LANs," in *Proc. IEEE INFOCOM - IEEE Conf. Comput. Commun.*, Toronto, ON, Canada, Apr. 2014, pp. 2463–2471.

[2] M. Mollanoori and M. Ghaderi, "Uplink scheduling in wireless networks with successive interference cancellation," *IEEE Trans. Mobile Comput.*, vol. 13, no. 5, pp. 1132–1144, May 2014.

[3] D. Jaramillo-Ramirez, M. Kountouris, and E. Hardouin, "Successive interference cancellation in downlink cooperative cellular networks," in *Proc. IEEE Int. Conf. Commun. (ICC)*, Sydney, NSW, Australia, Jun. 2014, pp. 5172–5177.

[4] J. He, Z. Tang, Z. Ding, and D. Wu, "Successive interference cancellation and fractional frequency reuse for LTE uplink communications," *IEEE Trans. Veh. Technol.*, vol. 67, no. 11, pp. 10528–10542, Nov. 2018.

[5] A. Goldsmith, "On the optimality of multiantenna broadcast scheduling using zero-forcing beamforming," *IEEE J. Sel. Areas Commun.*, vol. 24, no. 3, pp. 528–541, Mar. 2006.

[6] V. R. Cadambe and S. A. Jafar, "Interference alignment and spatial degrees of freedom for the K user interference channel," in *Proc. IEEE Intl. Conf. Commun. (ICC)*, Beijing, China, Jun. 2008, pp. 971–975.

[7] S. Mohajer, S. N. Diggavi, C. Fragouli, and D. Tse, "Transmission techniques for relay-interference networks," in *Proc. 46th Annu. Allerton Conf. Commun., Control, Comput.*, Monticello, IL, USA, Sep. 2008, pp. 467–474.

[8] Z. Li, J. Chen, L. Zhen, S. Cui, K. G. Shin, and J. Liu, "Coordinated multi-point transmissions based on interference alignment and neutralization," *IEEE Trans. Wireless Commun.*, vol. 18, no. 7, pp. 3347–3365, Jul. 2019.

[9] Y. Cao, S. Xu, J. Liu, and N. Kato, "IRS backscatter enhancing against jamming and eavesdropping attacks," *IEEE Internet Things J.*, vol. 10, no. 12, pp. 10740–10751, Jun. 2023.

[10] C. Masouros and E. Alsusa, "Dynamic linear precoding for the exploitation of known interference in MIMO broadcast systems," *IEEE Trans. Wireless Commun.*, vol. 8, no. 3, pp. 1396–1404, Mar. 2009.

[11] Z. Li, J. Chen, K. G. Shin, and J. Liu, "Interference recycling: Exploiting interfering signals to enhance data transmission," in *Proc. IEEE Conf. Comput. Commun. (INFOCOM)*, Paris, France, Apr. 2019, pp. 100–108.

[12] T. J. Cui, M. Q. Qi, X. Wan, J. Zhao, and Q. Cheng, "Coding metamaterials, digital metamaterials and programmable metamaterials," *Light: Sci. Appl.*, vol. 3, no. 10, p. e218, Oct. 2014.

[13] E. C. Strinati et al., "Wireless environment as a service enabled by reconfigurable intelligent surfaces: The RISE-6G perspective," in *Proc. Joint Eur. Conf. Netw. Commun. 6G Summit (EuCNC/6G Summit)*, Porto, Portugal, Jun. 2021, pp. 562–567.

[14] Q. Wu and R. Zhang, "Towards smart and reconfigurable environment: Intelligent reflecting surface aided wireless network," *IEEE Commun. Mag.*, vol. 58, no. 1, pp. 106–112, Jan. 2020.

[15] X. Pang, M. Sheng, N. Zhao, J. Tang, D. Niyato, and K. Wong, "When UAV meets IRS: Expanding air-ground networks via passive reflection," *IEEE Wireless Commun.*, vol. 28, no. 5, pp. 164–170, Oct. 2021.

[16] C. Zhao, X. Pang, W. Lu, Y. Chen, N. Zhao, and A. Nallanathan, "Energy efficiency optimization of IRS-assisted UAV networks based on statistical channels," *IEEE Wireless Commun. Lett.*, vol. 12, no. 8, pp. 1419–1423, Aug. 2023.

[17] H. Yang et al., "Intelligent reflecting surface assisted anti-jamming communications: A fast reinforcement learning approach," *IEEE Trans. Wireless Commun.*, vol. 20, no. 3, pp. 1963–1974, Mar. 2021.

[18] X. Tang, D. Wang, R. Zhang, Z. Chu, and Z. Han, "Jamming mitigation via aerial reconfigurable intelligent surface: Passive beamforming and deployment optimization," *IEEE Trans. Veh. Technol.*, vol. 70, no. 6, pp. 6232–6237, Jun. 2021.

[19] X. Pang, N. Zhao, J. Tang, C. Wu, D. Niyato, and K. Wong, "IRS-assisted secure UAV transmission via joint trajectory and beamforming design," *IEEE Trans. Commun.*, vol. 70, no. 2, pp. 1140–1152, Feb. 2022.

[20] T. Jiang and W. Yu, "Interference nulling using reconfigurable intelligent surface," *IEEE J. Sel. Areas Commun.*, vol. 40, no. 5, pp. 1392–1406, May 2022.

[21] Q. Wu et al., "Intelligent reflecting surface-aided wireless communications: A tutorial," *IEEE Trans. Commun.*, vol. 69, no. 5, pp. 3313–3351, May 2021.

[22] W. Tang et al., "Wireless communications with reconfigurable intelligent surface: Path loss modeling and experimental measurement," *IEEE Trans. Wireless Commun.*, vol. 20, no. 1, pp. 421–439, Jan. 2021.

[23] C. M. Yetis, T. Gou, S. A. Jafar, and A. H. Kayran, "On feasibility of interference alignment in MIMO interference networks," *IEEE Trans. Signal Process.*, vol. 58, no. 9, pp. 4771–4782, Sep. 2010.

[24] J. Chen, A. Singh, P. Elia, and R. Knopp, "Interference neutralization for separated multiuser uplink-downlink with distributed relays," in *Proc. Inf. Theory Appl. Workshop*, La Jolla, CA, USA, Feb. 2011, pp. 1–9.

[25] D. Wu, C. Yang, T. Liu, and Z. Xiong, "Feasibility conditions for interference neutralization in relay-aided interference channel," *IEEE Trans. Signal Process.*, vol. 62, no. 6, pp. 1408–1423, Mar. 2014.

[26] E. Basar and I. Yildirim, "Reconfigurable intelligent surfaces for future wireless networks: A channel modeling perspective," *IEEE Wireless Commun.*, vol. 28, no. 3, pp. 108–114, Jun. 2021.

[27] H. Jiang, B. Xiong, H. Zhang, and E. Basar, "Hybrid far-and near-field modeling for reconfigurable intelligent surface assisted V2V channels: A sub-array partition based approach," *IEEE Trans. Wireless Commun.*, vol. 22, no. 11, pp. 8290–8303, Nov. 2023.

[28] *Evolved Universal Terrestrial Radio Access (E-UTRA); Further Advancements for E-UTRA Physical Layer Aspects*, 3rd General Partnership Project (3GPP), document TR 36.814 R11 V9.2.0, 2017.

[29] I. F. Akyildiz, D. M. Gutierrez-Estevez, R. Balakrishnan, and E. Chavarria-Reyes, "LTE-advanced and the evolution to beyond 4G (B4G) systems," *Phys. Commun.*, vol. 10, pp. 31–60, Mar. 2014.

[30] C. You, B. Zheng, and R. Zhang, "Channel estimation and passive beamforming for intelligent reflecting surface: Discrete phase shift and progressive refinement," *IEEE J. Sel. Areas Commun.*, vol. 38, no. 11, pp. 2604–2620, Nov. 2020.

[31] S. Lin, M. Wen, and F. Chen, "Cascaded channel estimation using full duplex for IRS-aided multiuser communications," in *Proc. IEEE Wireless Commun. Netw. Conf. (WCNC)*, Austin, TX, USA, Apr. 2022, pp. 375–380.

[32] S. Ahmadi, *LTE-Advanced: A Practical Systems Approach to Understanding 3GPP LTE Releases 10 and 11 Radio Access Technologies*. New York, NY, USA: Academic, 2013.

[33] X. Ge, H. Cheng, M. Guizani, and T. Han, "5G wireless backhaul networks: Challenges and research advances," *IEEE Netw.*, vol. 28, no. 6, pp. 6–11, Nov. 2014.

[34] U. Siddique, H. Tabassum, E. Hossain, and D. I. Kim, "Wireless backhauling of 5G small cells: Challenges and solution approaches," *IEEE Wireless Commun.*, vol. 22, no. 5, pp. 22–31, Oct. 2015.

[35] X. Pang, W. Mei, N. Zhao, and R. Zhang, "Intelligent reflecting surface assisted interference mitigation for cellular-connected UAV," *IEEE Wireless Commun. Lett.*, vol. 11, no. 8, pp. 1708–1712, Aug. 2022.

[36] Z. Li, Y. Liu, K. G. Shin, J. Liu, and Z. Yan, "Interference steering to manage interference in IoT," *IEEE Internet Things J.*, vol. 6, no. 6, pp. 10458–10471, Dec. 2019.

[37] H. Salman, M. B. Janjua, and H. Arslan, "Improving connectivity via multi-user scheduling in 5G and beyond networks," in *Proc. IEEE Wireless Commun. Netw. Conf. (WCNC)*, Nanjing, China, Mar. 2021, pp. 1–6.

[38] T. Q. S. Quek and G. de la Roche, *Small Cell Networks: Deployment, PHY Techniques, and Resource Management*. New York, NY, USA: Cambridge Univ. Press, 2013.

Zhao Li (Member, IEEE) received the B.S. degree in telecommunications engineering and the M.S. and Ph.D. degrees in communication and information systems from Xidian University, Xi'an, China, in 2003, 2006, and 2010, respectively. He was a Visiting Scholar and then a Research Scientist with the Real-Time Computing Laboratory, Department of Electrical Engineering and Computer Science, University of Michigan, from 2013 to 2015. He is currently an Associate Professor with the School of Cyber Engineering, Xidian University. He has published over 40 technical papers at premium international journals and conferences, such as IEEE INTERNET OF THINGS JOURNAL, IEEE TRANSACTIONS ON WIRELESS COMMUNICATIONS, IEEE INFOCOM, IEEE TRANSACTIONS ON VEHICULAR TECHNOLOGY, and *Computer Communications*. His research interests include wireless communication, 5G communication systems, resource allocation, interference management, the IoT, and physical layer security.

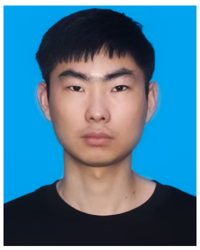

Chengyu Liu is currently pursuing the master's degree with the School of Cyber Engineering, Xidian University. His research interests include physical layer security and interference management.

Lijuan Zhang is currently pursuing the master's degree with the School of Cyber Engineering, Xidian University. Her research interests include wireless communication, physical layer security, and interference management.

Kang G. Shin (Life Fellow, IEEE) photograph and biography not available at the time of publication.

Jia Liu (Senior Member, IEEE) received the Ph.D. degree from the School of Systems Information Science, Future University Hakodate, Japan, in 2016. He is currently an Assistant Professor with the Center for Cybersecurity Research and Development, National Institute of Informatics (NII), Tokyo, Japan, and an Associate Professor with the School of Computer Science and Technology, Xidian University. He has published over 40 academic papers at premium international journals and conferences, such as IEEE TRANSACTIONS ON WIRELESS COMMUNICATIONS, IEEE TRANSACTIONS ON INFORMATION FORENSICS AND SECURITY, and IEEE INFOCOM. His research interests include wireless systems security, covert communications, and 5G. He received the 2016 IEEE Sapporo Section Encouragement Award.

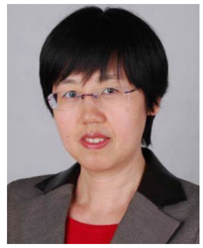

Zheng Yan (Fellow, IEEE) received the B.Eng. degree in electrical engineering and the M.Eng. degree in computer science and engineering from Xi'an Jiaotong University, Xi'an, China, in 1994 and 1997, respectively, the M.Eng. degree in information security from the National University of Singapore, Singapore, in 2000, and the Licentiate of Science and the Doctor of Science degrees in technology in electrical engineering from the Helsinki University of Technology, Helsinki, Finland, in 2005 and 2007, respectively. She is currently a Professor with Xidian University, Xi'an, and a Visiting Professor with Aalto University, Espoo, Finland. She authored more than 150 peer-reviewed publications and solely authored two books. She is the inventor and co-inventor of over 50 patents and PCT patent applications. Her research interests include trust, security and privacy, social networking, cloud computing, networking systems, and data mining. She served as a steering, organization, and program committee member for over 70 international conferences. She serves as an Associate Editor for *Information Sciences*, *Information Fusion*, IEEE INTERNET OF THINGS JOURNAL, IEEE ACCESS, *JNCA*, and *Security and Communication Networks*. She is the leading Guest Editor of many reputable journals, including *ACM TOMM*, *FGCS*, IEEE SYSTEMS JOURNAL, and *MONET*.

Riku Jäntti (Senior Member, IEEE) received the M.Sc. degree (Hons.) in electrical engineering and the D.Sc. degree (Hons.) in automation and systems technology from the Helsinki University of Technology (TKK) in 1997 and 2001, respectively. He is currently a Full Professor of communications engineering and the Head of the Department of Communications and Networking, School of Electrical Engineering, Aalto University, Finland. Prior to joining Aalto (formerly known as TKK) in August 2006, he was a Professor Pro Tem with the Department of Computer Science, University of Vaasa. His research interests include machine type communications, disaggregated radio access networks, backscatter communications, quantum communications, and radio frequency inference. He is a member of the Editorial Board of IEEE TRANSACTIONS ON COGNITIVE COMMUNICATIONS AND NETWORKING. He has been a IEEE VTS Distinguished Lecturer (Class 2016).